A Critical Look at Direct Catalytic Hydrogenation of Carbon Dioxide to Olefins

Ronda-Lloret, M.; Rothenberg, G.; Shiju, N.R.

DOI
10.1002/cssc.201900915

Publication date
2019

Document Version
Final published version

Published in
ChemSusChem

ChemPubSoc Europe
DOI: 10.1002/cssc.201900915
CHEMSUSCHEM Reviews

A Critical Look at Direct Catalytic Hydrogenation of Carbon Dioxide to Olefins

Maria Ronda-Lloret, Gadi Rothenberg, and N. Raveendran Shiju*[a]

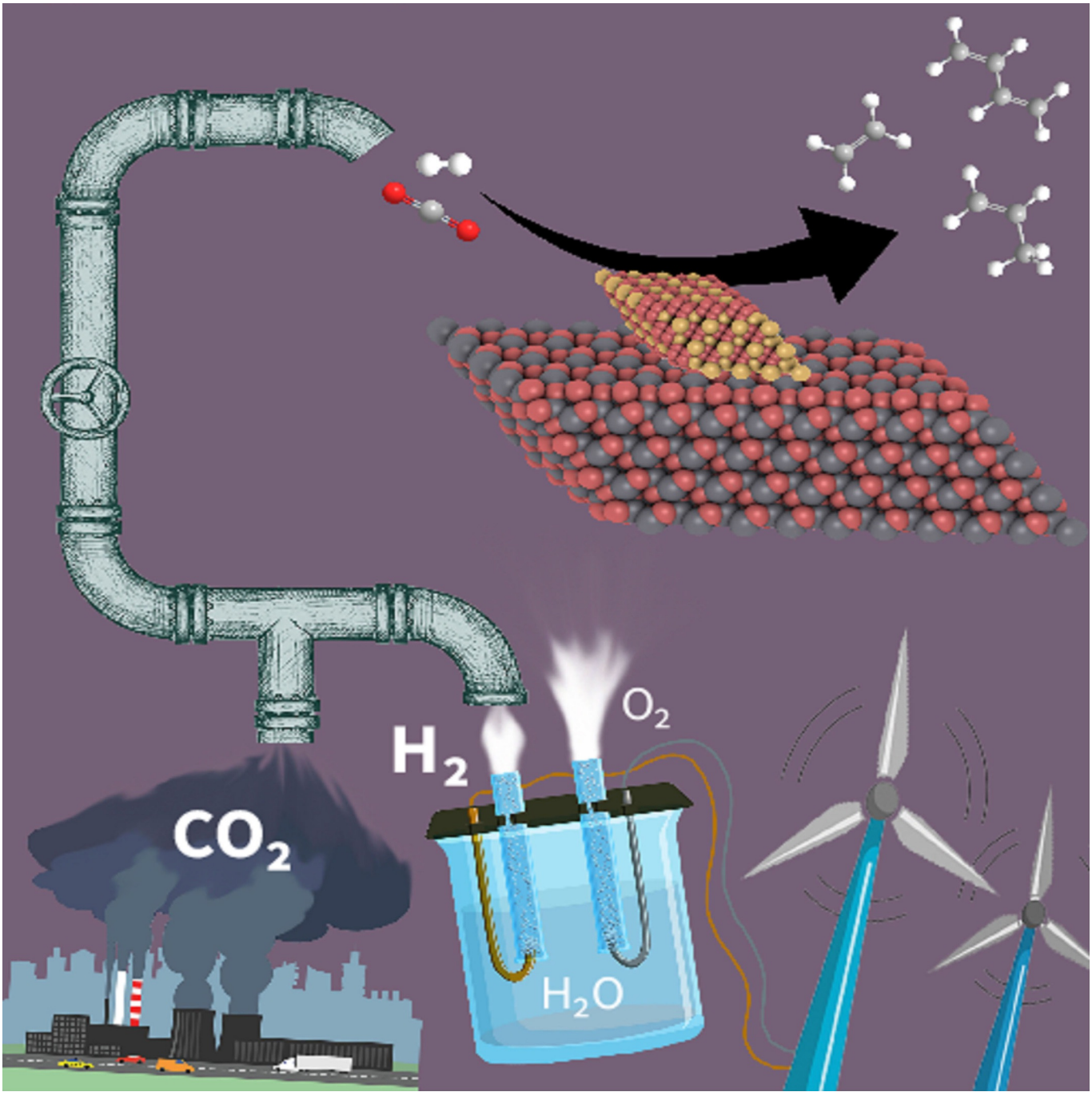

One of the main initiatives for fighting climate change is to use carbon dioxide as a resource instead of waste. In this respect, thermocatalytic carbon dioxide hydrogenation to high-added-value chemicals is a promising process. Among the products of this reaction (alcohols, alkanes, olefins, or aromatics), light olefins are interesting because they are building blocks for making polymers, as well as other important chemicals. Olefins are mainly produced from fossil fuel sources, but the increasing demand of plastics boosts the need to develop more sustainable synthetic routes. This review gives a critical overview of the most recent achievements in direct carbon dioxide hydrogenation to light olefins, which can take place through two competitive routes: the modified Fischer–Tropsch synthesis and methanol-mediated synthesis. Both routes are compared in terms of catalyst development, reaction performance, and reaction mechanisms. Furthermore, practical aspects of the commercialization of this reaction, such as renewable hydrogen production and carbon dioxide capture, compression, and transport, are discussed. It is concluded that, to date, the catalysts used in the carbon dioxide hydrogenation reaction give a wide product distribution, which reduces the specific selectivity to lower olefins. More efforts are needed to reach better control of the C/H surface ratio and interactions within the functionalities of the catalyst, as well as understanding the reaction mechanism and avoiding deactivation. Renewable H_2 production and carbon dioxide capture and transport technologies are being developed, although they are currently still too expensive for industrial application.

1. Introduction

The increasing amount of anthropogenic carbon dioxide (CO_2) emissions is a global concern. There is a correlation between the rise in global temperatures and the rise in atmospheric CO_2 concentration levels (Figure 1).[1] Even if this does not imply direct causality, mankind cannot afford to take chances. This feeling is echoed in the 2015 Paris Agreement, which shows the willingness of policy experts, scientists, and climate economists from 118 countries to take measures to fight climate change. Its main goal is to keep the increase in global average temperature below 2 °C and ultimately achieve net-zero emissions of greenhouse gases (GHGs).[2,3]

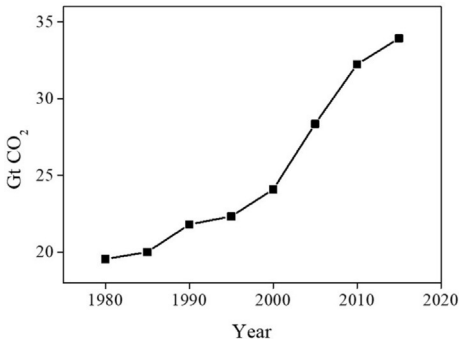

Figure 1. World CO_2 net emissions from 1980 to 2015.[4]

This goal is feasible, yet difficult. Reducing the amount of CO_2 in the atmosphere could reduce the greenhouse effect, but this requires individuals and companies to change their behavior, which, in turn, requires economic and social incentives. Controlling the carbon footprint and higher taxes on carbon emissions or on fossil fuels are some examples. The main sources of CO_2 are power generation and manufacturing (Table 1). Moving away from fossil fuels to cleaner energy sources remains a big challenge.

Table 1. Total CO_2 emissions by sector from 1980 to 2015.[4]

Sector	CO_2 source	Emissions [Gt]
electricity	carbon-based power plants	12.4
heavy industry	production of cement, limestone, and hydrogen	3.9
transport	road > air > ship > rail	6.0 > 0.9 > 0.8 > 0.1

Developed countries are starting to act in terms of renewables and natural gas to reduce emissions. For example, according to the European Environmental Agency (EEA), in 2016, Europe avoided the emission of 460 Mt of CO_2 through the use of renewable energy.[5] The main renewable energy sources are on- and offshore wind power and solar photovoltaics for electricity generation, as well as solid biomass-based technologies for heating and cooling.[5,6] In addition, the EU remains a world leader in renewable power, with 0.87 kW of renewable energy capacity installed per person in 2017, followed by the USA (0.71 kW/person) and Brazil (0.61 kW/person).[5] Nevertheless, the use of coal and its technology remains well established. In 2017, a net capacity of 35 GW of coal-fired generation was added to the global fleet.[5] The gross addition was 67 GW (mainly in developing economies) and the capacity retired was 32 GW (mainly in the USA and Europe).[5] If we look into areas under fast economic development, such as South-East Asia, we see that coal usage is increasing, especially with the commissioning of numerous coal-fired power plants since 2000.[3,7] Upon examining the magnitude and distribution of the world energy demand, it appears that coal, oil, and natural gas will remain our main energy sources in the next 50 years. Changing this large-scale trend is possible only through a combination of economically viable alternatives and strong regulations.

[a] *M. Ronda-Lloret, Prof. Dr. G. Rothenberg, Dr. N. R. Shiju*
van 't Hoff Institute for Molecular Sciences
University of Amsterdam, Science Park 904
1090 GD Amsterdam (The Netherlands)
E-mail: n.r.shiju@uva.nl

The ORCID identification number(s) for the author(s) of this article can be found under:
https://doi.org/10.1002/cssc.201900915.

Shiju Raveendran is Associate Professor at the University of Amsterdam. He obtained his Ph.D. in catalysis from the National Chemical Laboratory, Pune, India. After postdoctoral stays in the UK and USA, he joined the University of Amsterdam as a faculty member in 2009. In 2010, he won the Amsterdam Science Park Ideas Prize for the discovery of a new catalyst. One of his patents was sold to industry in 2012. He is a board member of the Dutch Zeolite Association and an editorial board member of *FlatChem* and *EnergyChem*; two new journals by Elsevier. His research interests include CO_2 conversion, biomass conversion, and lower alkane activation. He is also developing renewable jet fuel from organic waste with the support of http://booking.com.

Maria Ronda-Lloret graduated from the University of Alicante (Spain) with a B.Sc. degree in chemistry (2015) and an M.Sc. degree in materials science (2016). During her master's thesis in the Advanced Materials Laboratory, she worked on the synthesis of metal–organic frameworks and their application in heterogeneous catalysis. She is currently a Ph.D. student in the Heterogeneous and Sustainable Chemistry group at the University of Amsterdam. Her Ph.D. work focuses on the development of novel catalysts for CO_2 conversion reactions, such as the dry reforming of butane and the reverse water–gas shift, by using both thermal and plasma reactors.

Gadi Rothenberg was born in Jerusalem in 1967, and immediately (well, 26 years later) was awarded a B.Sc. in chemistry magna cum laude from the Hebrew University of Jerusalem. Instead of getting a real job, he continued for a Ph.D. summa cum laude in applied chemistry (1999) and decided to become an academic. Since 2008 he is Professor and Chair of Heterogeneous Catalysis and Sustainable Chemistry at the University of Amsterdam. He teaches courses on catalysis and workshops on scientific writing and innovation. In addition to publishing two books and over 200 papers in peer-reviewed journals, he has also invented 16 patents and co-founded the companies Sorbisense, Yellow Diesel, and Plantics.

Scientists have been studying methods for reducing CO_2 emissions for decades. Capturing CO_2, either from flue gases of industrial processes or directly from the atmosphere, is one such option. Yet, carbon capture and storage (CCS) presents technical and economic barriers. CO_2 leakage rates are uncertain and there are limits in storage capacity, depending on location. Moreover, CCS requires strong regulatory incentives because it does not produce any intrinsic value.[8] Perhaps the strongest argument against CCS, however, is that it basically considers CO_2 as garbage. This is not a good chemical solution. Instead, we should consider CO_2 as a resource and aim for carbon capture and utilization (CCU). If we could use CO_2 as a raw material to make profitable products, governments and companies would be encouraged to follow suit. The basic technology is already in place, by using the adsorption of CO_2 in solvents such as monoethanolamine (MEA) to give carbamates.[8] During post-combustion capture, flue gases, including CO_2, are bubbled through a solution in MEA. CO_2 is then recovered by heating the carbamate solution.[9] Afterwards, CO_2 is cleaned (and dried if necessary) and compressed for transport and utilization. This method still has drawbacks regarding the energy penalty of the MEA regeneration process. Other amine solvents are being researched, as well as physical absorption processes by using solid adsorbents, such as activated carbons, molecular sieves, zeolites, and polymers.[10] After capture or separation of CO_2, efforts are being made to efficiently convert CO_2 into high-value-added products, such as fuels and chemical feedstock. Converting CO_2 into urea (for fertilizers) and the production of plastics, such as polycarbonates, are performed today.[3,11] Methanol synthesis is industrially achieved from a mixture of CO_2, CO, and H_2.[12] However, methanol is nowadays also obtained from CO_2. For example, Carbon Recycling International (CRI) developed the world's first commercial CO_2 to methanol plant in Iceland. The George Olah Renewable Methanol Plant now recycles 5500 tonnes of carbon.[13]

Catalytic CO_2 conversion to high-value-added chemicals can be achieved through different methods. The electrocatalytic pathway has mainly focused on the CO_2 reduction reaction (CO_2RR) to hydrocarbons, as well as to CO and alcohols. This process is already close to commercialization, but its economic viability depends strongly on the cost of electricity.[14] Another alternative is photocatalysis, typically with semiconductor catalysts, which can enable direct solar to fuel conversion. Although photocatalysis is independent of an electricity source, its efficiency is still too low for industrial applications.[15] Plasma and plasma catalytic reactions are also gaining attention, especially CO_2 splitting and dry reforming of methane (DRM).[16–18] Thermocatalytic CO_2 conversion is also well known. For instance, DRM with CO_2 is used to produce syngas, which is then used for the production of hydrocarbons or alcohols through the Fischer–Tropsch synthesis (FTS).[16] The thermocatalytic hydrogenation of CO_2 is interesting because of different products that can be obtained. These are mainly alkanes (liquefied petroleum gas and gasoline), alkenes, and aromatics.

Alkenes (olefins) are divided in two subgroups: lower olefins ($C_2^=$–$C_4^=$) and higher olefins ($C_{5+}^=$). Higher olefins, in particular, linear α-olefins, are important industrial intermediates for pro-

ducing polyvinyl chloride (PVC) plasticizers, synthetic lube oils, detergents, and surfactants.[19,20]

Lower olefins ($C_2^=$–$C_4^=$), generally referring to ethylene, propylene, butylene, and 1,3-butadiene, are important chemicals because they are the building blocks of plastics, synthetic textiles, rubbers, solvents, and coatings.[21] In particular, a summary of the most important chemicals is as follows:

1) Ethylene is one of the most important feedstocks in the chemical industry. In the plastics sector, it is mainly used for the production of polyethylene, but also other plastics, such as polyethylene terephthalate (PET) and PVC.[21,22] It is also used for producing intermediate chemicals, such as ethylbenzene, ethylene oxide, and ethylene chloride.
2) Propylene is mainly used for the production of polypropylene (PP), as well as propylene oxide (plastics) and cumene (solvents production).[21]
3) The most important C_4 olefin is 1,3-butadiene. It is the key monomer for producing styrene butadiene rubber (SBR), which is the main component of car tires. Butadiene is also used to make adiponitrile, as well as acrylonitrile–butadiene–styrene (ABS), polybutadiene, styrene–butadiene (SB) latex, and nitrile rubbers (NBRs).[23] The other butenes are used mainly in the fuel industry. Isobutylene is a raw material for the synthesis of methyl *tert*-butyl ether (MTBE) and ethyl *tert*-butyl ether (ETBE), which are used as octane enhancers in gasoline. Linear butenes are used for synthesizing methyl ethyl ketone (MEK) as well as higher olefins.[21]

Traditionally, light olefins are obtained as products of the cracking of naphtha in the oil refinery industry.[24,25] Plastic production from fossil fuels increased from 15 million tonnes in 1964 to 311 million tonnes in 2014.[26] Yet, even this will not cover the increasing demand of olefins for plastics due to the projected expansion of the middle classes in the next two decades, especially in Asia.[23] Furthermore, olefin production itself incurs large CO_2 emissions. Between 0.18 and 0.2 Gt of CO_2 emissions worldwide were estimated to be produced by olefin production in 2000.[27,28] If we desire a future with net-zero emissions, we must find other carbon sources for producing olefins. The production of olefins from CO_2 is then a promising option. The 34 Gt of CO_2 emitted in 2015[4] is equivalent to 9.3 Gt of carbon. Thus, one could produce 0.46 Gt of ethylene from captured CO_2, even if the efficiency of the process was only 10%. For comparison, the global ethylene demand in 2011 was "only" 0.13 Gt.[21] The production of olefins from CO_2 would not solve the entire problem of CO_2 emissions, but it would avoid part of the emissions produced by traditional cracking processes while expanding olefin production capacity.

However, to use CO_2 in any chemical process, we must overcome its high thermodynamic stability, $\Delta G^0 = -394.4\ kJ\,mol^{-1}$, which usually means high reaction temperatures. One way around this problem is to use a high-energy coreactant.[11] For this purpose, hydrogen is a good candidate. With the right catalysts, CO_2 hydrogenation can produce a mixture of light olefins, higher olefins, and alkanes. The desired olefins can then be separated from the mixture, for example, by using membranes.[29,30]

There are several recent and good reviews on CO_2 hydrogenation.[31–39] These typically focus on the production of hydrocarbons, rather than on olefins. Interest in CO_2 hydrogenation to olefins has been increasing, and several reviews have focused on this topic.[40,41] Moreover, increasing interest in CO_2 hydrogenation means that many new research results are published and almost on a daily basis (over 1400 studies were published on CO_2 hydrogenation in 2017–2018, ca. 2 papers per day). Here we provide an overview on the catalytic hydrogenation of CO_2 to olefins, emphasizing studies since 2017. We discuss reaction pathways, reaction conditions, active catalysts, and possible mechanisms. We also include a section on practical aspects of the commercialization process.

2. The CO_2 Hydrogenation Reaction

CO_2 hydrogenation can take place through two competing pathways: the modified Fischer–Tropsch synthesis (MFTS) and the methanol-mediated synthesis (see Scheme 1). These pathways are distinguished by their intermediates: in the first route, CO_2 is reduced to CO through reverse water gas shift

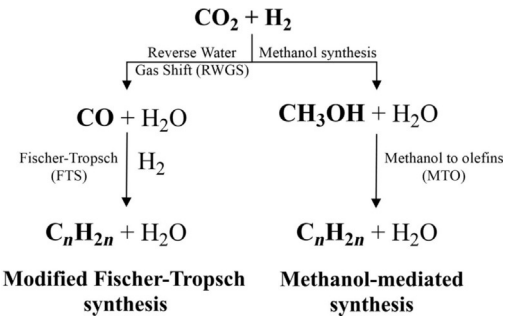

Scheme 1. Direct routes for the production of olefins by CO_2 hydrogenation.

(RWGS), followed by chain propagation through FTS. In the second route, CO_2 is hydrogenated first to methanol and then converted into hydrocarbons. In both routes, it is the chain propagation step that generates value-added hydrocarbons. The reaction conditions and catalysts can be tuned towards different products, including liquefied petroleum gas (C_3–C_4^0), lower olefins (C_2–$C_4^=$), gasoline (C_5–C_{11}), or aromatics.

Because both routes involve two different steps, a two-stage reactor can be used (the indirect route). In this way, the two steps can run by using two different catalysts and under specific reaction conditions that are optimized for each step. Yet, because the two steps are not mutually exclusive, direct routes with a single reactor are also possible. The direct catalytic hydrogenation of CO_2 to olefins in a single reactor makes sense. It is potentially more economical and energy-efficient, which is crucial for process viability.[42] For this reason, we focus on recent developments for this direct route.

2.1. Catalytic CO_2 hydrogenation through the MFTS route

2.1.1. The reaction

The MFTS route combines RWGS and FTS. The first step is an equilibrium reaction [Eq. (1)]. This reaction is endothermic and requires elevated temperatures.[33] It is also sensitive to the actual C/H ratio on the surface. Because CO_2 has a lower adsorption strength than that of H_2, the fast hydrogenation of carbon species adsorbed on the surface is favored, leading to the formation of the unwanted methane byproduct.[43] CO produced by RWGS is then hydrogenated in FTS [Eq. (2)].

$$CO_2 + H_2 \rightleftharpoons CO + H_2O,\ \Delta H_{25\,^\circ C} = 41.2\,kJ\,mol^{-1} \quad (1)$$

$$n\,CO + 2n\ H_2 \rightleftharpoons C_nH_{2n} + n\,H_2O \quad (2)$$

In practice, Equation (2) is a multistep process: reactant adsorption, chain initiation, chain growth, chain termination, and product desorption.[44] Looking at the overall process (RWGS + FTS), RWGS is an endothermic reaction and FTS reactions are exothermic. Reaction conditions (temperature, pressure, H_2/CO_2 ratio) will affect CO_2 conversion and product distribution. This requires a compromise in the reaction conditions. Yao et al. analyzed the thermodynamics of this system.[45] They found that, below 500 °C, long-chain olefins were favored at lower temperatures and short-chain olefins were favored at higher temperatures. Temperatures of around 400 °C were suitable for the synthesis of light olefins. However, this study does not take into account the formation of alkanes.

The product distribution in FTS can be described by the Anderson–Schulz–Flory (ASF) theory, which models the chain growth probability, depending on the operating conditions and catalyst. This is represented by the α factor, which indicates the probability that a CO/CO_2 atom molecule will react to extend the hydrocarbon chain. In practice, a multicomponent product mixture is formed. ASF is useful only as an approximation.[44] Upon changing the feed gas composition from CO/H_2 to CO_2/H_2, the product distribution changes significantly. Under these conditions, some catalysts do not fit to the ASF product distribution.[46] Because the α factor is not reported in all CO_2 hydrogenation studies, we focus herein on CO_2 conversion and the ratio of olefins/paraffins (O/P) as indicators of catalyst performance.

2.1.2. The catalysts

Reviews by Yang et al.[36] and Li et al.[37] focus on the production of value-added hydrocarbons, covering both alkanes and olefins. Ma and Porosoff recently published a review focused on the use of tandem catalysts in this reaction.[40] In addition, Wang et al. gave a short overview of the aspects of this reaction, mainly by the MFTS route.[41] Herein, we only focus on olefin production and on the fundamental aspects of the reaction. With this, we aim to clarify which catalysts are suitable for obtaining olefins from the MFTS CO_2 hydrogenation route. Because MFTS involves two steps, the optimal catalyst must be active in both RWGS (CO_2 activation) and FTS chain growth (C–C bond formation). Herein, we see that MFTS catalysts are based on FTS catalysts.

Iron-based catalysts

Iron-based catalysts are those most commonly used for CO_2 hydrogenation through the MFTS route, thanks to their good performance in FTS and the water gas shift (WGS) reaction.[21] Under FTS conditions, these catalysts form coexisting phases, including metallic iron (α-Fe), iron oxides (α-Fe_2O_3, Fe_3O_4), and iron carbides (χ-Fe_5C_2).[47] The effect of each phase on the catalytic activity is unclear because the phases themselves can change during the reaction. Previous work showed that the active phase for RWGS was the oxide Fe_3O_4,[48] whereas for the FTS step it was the carbide χ-Fe_5C_2.[49] Modified iron catalysts were developed for CO_2 hydrogenation. Either unsupported catalysts or iron supported on Al_2O_3, ZrO_2, CeO_2, metal–organic frameworks (MOFs) and carbon supports were tested. Alkali-metal promoters are usually added to enhance the selectivity towards olefins, but the effect of adding a second metal (Cu, Mn, Zn) has also been studied.

The effect of dopants and supports on the CO_2 hydrogenation ability of iron-based catalysts was widely studied. However, fewer studies focused on improving the performance of pristine iron catalysts. A cellulose-templated synthesis method and the use of ammonium glycolate complexes were studied. Although they showed promising results, the addition of a promoter was needed to perform the reaction selectively.[50,51]

Alkali-metal cocatalysts

Adding alkali metals (K^+, Na^+, Rb^+, Cs^+, and Li^+) to iron-based catalysts improves both CO_2 conversion and olefin production, mainly because of their electronic and basic properties. Adding potassium as a basic promoter is an established practice. It enhances the adsorption of CO_2 molecules on the catalyst surface. This can increase CO_2 conversion. Furthermore, because CO_2 adsorption increases, the hydrogenation ability of the promoted catalyst decreases.[52] This results in a lower H/C ratio on the surface, and less methane is formed. The formation of C_2–$C_4^=$ is also favored due to the electronic properties of alkali metals. The presence of K^+ on the catalyst surface may hinder the readsorption of olefins (both electron donors), and thus, avoid the hydrogenation of double bonds and production of saturated hydrocarbons.[53] Adding K^+ can also affect the type and concentration of iron carbides formed during the reaction. The formation of Hägg carbides (χ-Fe_5C_2) is accelerated if K^+ is used.

For example, in Fe/SiO_2 catalysts, the rate of carburization (reduction of FeO_x to carbide phase) increased in the order: unpromoted catalyst < Li^+ < Na^+ < K^+ ≈ Rb^+ ≈ Cs^+.[54] Recently, Wu et al. showed that iron catalysts supported on a 3D graphene called honeycomb-structured graphene (HSG) and promoted with potassium converted more CO_2 and gave higher selectivity towards C_2–$C_4^=$ than that of the unpromoted catalyst.[52] Mössbauer analysis of ^{57}Fe showed that the sample FeK1.5/HSG after the reaction contained more χ-Fe_5C_2 (74%)

and could stabilize an extra carbide phase, ε′-$Fe_{2.2}C$ (8.5%), compared with that of the unpromoted Fe/HSG catalyst (50.4% χ-Fe_5C_2). The change in electron density of iron species in the presence of K^+ might also affect the strength of the chemical bonds on the catalyst surface: the C–O bond in CO molecules can be weakened and the Fe–C bond can be strengthened to accelerate the formation of iron carbides.[54]

Copper-based catalysts

Copper is often used as a promoter to facilitate FeO_x reduction and carbidization to the Hägg iron carbide, as well as for promoting the dispersion of iron particles.[55] It is also used as an active site in the RWGS reaction, which inhibits methane production, in contrast with Co, Ni, and Ru.[33] Thus, adding copper enhances CO_2 conversion while keeping the product distribution constant. The correct Cu/Fe ratio is needed to obtain a positive effect from adding Cu. The addition of 10% Cu to a Fe–K/Al_2O_3 catalyst increased CO_2 conversion to 41%, relative to the unpromoted catalyst (24% of CO_2 conversion).[56] The obtained O/P ratio was 4.9, which was similar to that of the sample without Cu (4.3). Higher Cu loadings showed lower CO_2 conversion. Wang et al. found that the optimal Cu/(Cu + Fe) atomic ratio was 0.17, which corresponded to 17% total metal loading.[57] This bimetallic catalyst supported on Al_2O_3 reached the highest CO_2 conversion among all tested ratios. Its XRD pattern showed a new peak at 45°, which was ascribed to Fe–Cu alloy species. Because adding copper did not change the product distribution, potassium was also added. They observed a linear correlation between the O/P ratio and K/Fe atomic ratio.

Manganese and zinc cocatalysts

The promotion of iron-based catalysts with other transition metals, such as manganese or zinc, was also studied. Zinc acts as a structural promoter: it increases the surface area of the catalyst and improves the dispersion of iron active sites.[58,59] The introduction of ZnO clusters leads to highly dispersed and small Fe crystals, which increases the mass-specific activity. However, it also forms the $ZnFe_2O_4$ spinel phase, which is not reducible, and therefore, inactive.[60] Previous studies showed that higher Zn/Fe ratios decreased CO_2 conversion, but increased the amount of lower olefins in the product mixture by suppressing the formation of heavy products.[59] If Mn is coprecipitated with α-Fe_2O_3, some of the Fe^{3+} ions are replaced by Mn^{3+} ions, which gives an α-$(Fe_{1-x}Mn_x)_2O_3$ solid solution.[61]

The electronic effect of Mn and Zn is a controversial topic. In general, the surface basicity (usually determined by CO_2 uptake measurements) of the catalyst is higher upon adding Mn or Zn,[61] although there are exceptions.[59] Its effect on CO_2 conversion and olefin selectivity does not correlate with higher CO_2 conversion and/or olefin production.[62,63] Falbo et al. compared zinc- and manganese-containing bulk iron-based catalysts.[64] The former showed higher surface basicity, which slightly improved CO_2 conversion and increased the O/P ratio in the C_3–C_6 range. However, previous studies reported that Mn-doped catalysts showed better surface basicity than that of Zn-based catalysts.[61] A recent study by Wang et al. showed that the electronic effect of these metals strongly depended on the metal loading and preparation method.[65] Zn–Fe/K prepared by a coimpregnation method showed a higher CO_2 adsorption capability (higher basicity) than that of catalysts prepared by solvo- or hydrothermal methods. However, the catalytic differences were minor: the coimpregnated sample showed a slightly higher CO_2 conversion, but the O/P ratio was similar.

Cobalt-based catalysts

Cobalt-based catalysts are traditional FTS catalysts that show high activity and selectivity towards heavy hydrocarbons from syngas.[34] However, they are poor RWGS catalysts, and thus unsuitable for CO_2 hydrogenation. The C_2–C_4 hydrocarbon production is limited, with methane as main product.[66] Despite this, cobalt was used as dopant in Fe/K catalysts. Adding a small amount of Co (2.6 wt%) to a Fe (12.4 wt%) catalyst showed higher CO_2 conversion than an unpromoted Fe catalyst.[67] The addition of potassium remains essential to produce olefins. In another study, highly alkalized Co–Fe/K/Al_2O_3 catalyst (8.7 wt% of K) decreased the amount of weakly adsorbed H_2 and enhanced CO_2 adsorption, resulting in a decrease in the hydrogenation of produced olefins. This catalyst gave a 5.2 O/P ratio.[68] Another study showed higher O/P ratios if higher calcination temperatures were used during synthesis of the catalyst.[69] O/P ratios were up to 7.3 if calcined at 800 °C, at the expense of CO_2 conversion. At higher calcination temperatures, iron oxide particles are bigger and harder to reduce than that at lower calcination temperatures, which diminishes CO_2 conversion values. $KAlO_2$ species also form. These can suppress the further hydrogenation of the olefin products, increasing the O/P ratio. Although methane production is still considered to be an issue if using cobalt, the latest advances show that these catalysts can restrict the formation of CH_4 to 15% or less.[57,69]

Supported catalysts

Supports are useful for dispersing the active phase and avoiding agglomeration during the reaction. Many studies used γ-Al_2O_3 as a support, due to its high surface area and strong metal–support interactions that prevented sintering.[70] Yet, the strong metal–support interactions achieved with γ-Al_2O_3 might impede carbidization of iron species, lowering the catalytic activity of the material.[71] Other popular supports are SiO_2 and TiO_2,[33] whereas other studies showed that Fe–K catalysts with ZrO_2 as a support were more active for CO_2 hydrogenation than that with γ-Al_2O_3, SiO_2, or TiO_2.[53] This may be related to the surface basicity and its capability to adsorb CO_2. Redox-active supports, such as ceria, are also interesting because they can modify the properties of the catalyst without the use of promoters; thus facilitating the reduction of FeO_x species.[72] The appropriate amount of Ce in the Fe–Zr–K catalyst increased the surface basicity and decreased Fe_2O_3 particle

size.[73] Therefore, the dispersion of Fe active sites and their reducibility were enhanced. CO_2 conversion and olefin selectivity were improved to give O/P ratios up to seven.

Nontraditional supports, such as MOFs, have gained attention for CO_2 conversion due to their high surface area and large pore volumes.[74] Guo et al. reported the superior performance of catalysts formed by Fe_2O_3 being ground together with MIL-53(Al) or ZIF-8, compared with conventional Fe_2O_3/γ-Al_2O_3 or unsupported Fe_2O_3.[75] MIL-53(Al) showed a lower CO_2 activity and no formation of olefins due to its acidic properties. The O/P ratio with ZIF-8 was very small (0.2) compared with that reported in the literature, so further improvements in this type of catalyst are needed to compete with other iron-based catalysts. MOFs were also utilized as templates or precursors of porous carbon materials with nanostructured metal species through thermal decomposition. MIL-88(Fe) pyrolyzed at 600 °C was found to lead to the optimum Fe_3O_4/χ-Fe_5C_2 proportion.[71] This catalyst showed the lowest surface area and highest CO_2 conversion value than that with pyrolysis temperatures of 500 or 700 °C. Upon adding K^+, olefin production was significantly enhanced (O/P = 5.5). Although, in this case, the O/P values are higher, 20% CO and 25% CH_4 are reported, which decreases the suitability of MOFs and carbon-based materials for CO_2 hydrogenation. Improvements were achieved with regard to CO and CH_4 selectivity. Another iron-based MOF (BasoliteF300) was used as a template for the preparation of a Fe/C catalyst, which was promoted with potassium.[76] At 350 °C, the catalyst gave 38.5% CO_2 conversion with a C_2–C_6 olefin selectivity of 38.8%. In this study, the CO and CH_4 amounts decreased to 8 and 10%, respectively.

The amount of graphitic carbon also affects the olefin production rates. Gupta et al. studied the catalytic behavior of iron-based carbon-coated core–shell nanocatalysts.[77] They showed that, upon increasing the amount of carbon in the shell, the O/P ratio decreased. Graphitic carbon is known for its good ability of H_2 adsorption and mobility (spillover effect), leading to a higher production of methane and paraffins.[53]

Graphene (or reduced graphene oxide (rGO)) is an interesting carbon support due to its characteristics, such as large surface area and 2D structure.[78,79] Because metal–support interactions are moderate with carbon, iron catalysts can exhibit a high degree of reduction and carburization.[80] If rGO was tested as a support of Fe–K catalysts for the FTS reaction, it gave high O/P ratios (up to 11) with 67% selectivity towards olefins. The activity, expressed as moles of CO converted to hydrocarbons per gram Fe per second (iron time yield to hydrocarbons, FTY), was 220 $\mu mol_{CO}\, g_{Fe}^{-1}\, s^{-1}$.[80,81] The synthesis of olefins from CO_2 hydrogenation with rGO-based materials was also reported.[52] The same study also reported a novel 3D structure derived from HSG, which showed slightly better catalytic performance than that of rGO. This material is able to dissipate reaction heat, and therefore, impede the agglomeration of iron carbide nanoparticles. Despite the novel properties of this 3D structure, considerably higher CO and CH_4 selectivity values were reported. Table 2 compares the various MFTS-based catalysts and their performances.

2.1.3. Reaction mechanisms

As outlined above, the MFTS route is a two-step process. The CO_2 molecules dissociate in the RWGS step, producing CO, which is then hydrogenated in the FTS step. Several mechanisms were proposed for the RWGS and FTS individually; these were dependent on the nature of the catalyst used.

Two main mechanisms for the RWGS reaction were proposed: 1) the redox mechanism, and 2) the associative mechanism.[33] However, the actual route may well combine both pathways and differ between catalysts. Kinetic studies showed that, for a Fe–K/Al_2O_3 catalyst, a combination of redox and associative pathways occurs, with the redox mechanism dominating.[82] Scheme 2 shows the elementary reactions for each proposed mechanism. In the redox pathway, CO_2 adsorbs and dissociates on the reduced active sites, which leads to the oxidation of active sites. H_2 reduces the active sites back, which forms water. During the associative mechanism pathway, adsorbed CO_2 reacts with dissociated H_2 to form a surface intermediate (in this case, the main carbon-containing intermediate was detected by means of IR as formate). This intermediate de-

Table 2. A selection of some recent studies on CO_2 hydrogenation to lower olefins. Only results with CO_2 conversion values between 20 and 40% are shown.

Catalyst	X_{CO_2} [%]	Selectivity[a] [%]			O/P ratio[b]	Reaction conditions			Space velocity [mL $g_{cat.}^{-1}\, h^{-1}$]	Ref.
		CO	CH_4	$C_2^=$–$C_4^=$		T [°C]	H_2/CO_2 ratio	P [MPa]		
80 Fe20 Cu/K/Al_2O_3	30	5.7	9.2	n.r.[c]	5.5	300	3/1	2	756	[56]
Fe–Cu(0.17)/K(1)/Al_2O_3	29.3	17.0	7.0	n.r.	5.2	300	3/1	1.1	3600	[57]
Fe–Co/K/Al_2O_3	37.2	28.9	13.5	30.2	7.3	320	3/1	2	3600	[69]
5 Fe–1 Zr–1 Ce–K	28.2	10.5	41.8	22.6	1.1	320	3/1	2	n.r.	[73]
Fe/ZIF-8	30	17	25	8	0.2	300	3/1	3	3600	[75]
FeK1.5/rGO	37	46	n.r.	30.24	5.6	340	3/1	2	2200	[52]
$ZnGa_2O_4$/SAPO-34	37	85	0.8	6.8	1.0	450	3/1	3	5400	[95]
In–Zr/SAPO-34	35.5	85	0.6	11.5	4.6	400	3/1	3	9000	[93]
ZnZrO/SAPO	20	65	1.8	28	8	400	3/1	2	3600	[87]
In–Zr/SAPO-34	26.2	63.9	0.7	26.9	3.5	380	3/1	3	9000	[98]
CuZnZr@Zn-SAPO-34	19.6	58.6	6.1	25.0	3	400	3/1	2	n.r.	[106]

[a] The selectivity values in this table are calculated on a carbon basis, including CH_4, CO, C_2–C_4 olefins, C_2–C_4 alkanes, and C_{5+} compounds. [b] O/P ratio refers to the difference in olefins to paraffins in the product mixture. [c] n.r. refers to data that has not been reported.

Redox pathway	Associative pathway
1) $CO_2\,(g) + s \rightleftharpoons CO_2{\cdot}s$	1) $H_2\,(g) + s \rightleftharpoons H_2{\cdot}s$
2) $CO_2{\cdot}s + s \longrightarrow CO{\cdot}s + O{\cdot}s$	2) $H_2{\cdot}s + s \rightleftharpoons H{\cdot}s + H{\cdot}s$
3) $CO{\cdot}s \rightleftharpoons CO\,(g) + s$	3) $CO_2\,(g) + s \rightleftharpoons CO_2{\cdot}s$
4) $H_2\,(g) + O{\cdot}s \rightleftharpoons H_2O{\cdot}s$	4) $H_2{\cdot}s + CO_2{\cdot}s \longrightarrow COOH{\cdot}s + s$
5) $H_2O{\cdot}s \rightleftharpoons H_2O\,(g) + s$	5) $COOH{\cdot}s + H{\cdot}s \rightleftharpoons CO\,(g) + H_2O\,(g) + 2s$

Scheme 2. Redox (left) and associative (right) reaction pathways for the RWGS reaction.[82]

sorbs as CO and water. Other structures of carbon-containing intermediate were proposed, such as carbonate, carbonyl, or carboxylate species.

For iron-based catalysts, magnetite (Fe_3O_4) is usually considered as the active phase in RWGS. Fresh iron catalysts consist of α-Fe_2O_3 (hematite phase), and so catalysts are generally reduced prior to the reaction. Under a H_2 atmosphere, reduction to Fe_3O_4, FeO, or metallic iron (Fe^0) can take place. Under a syngas atmosphere, as well as a CO_2+H_2 atmosphere, all of these reduced iron species can convert into iron carbides, such as χ-Fe_5C_2, ε'-$Fe_{2.2}C$, and θ-Fe_3C (Scheme 3). The carburization ability follows the order $Fe_3O_4 < FeO < Fe^0$.[83]

The χ-Fe_5C_2 iron carbide, usually formed under reaction conditions, is considered to be the active phase for the FTS reaction, because hydrocarbon species are only detected after its formation.[83] Riedel et al. verified this by measuring how the product composition changed through time if a Fe–Al–Cu–K-containing catalyst was exposed to a H_2/CO_2 atmosphere.[84]

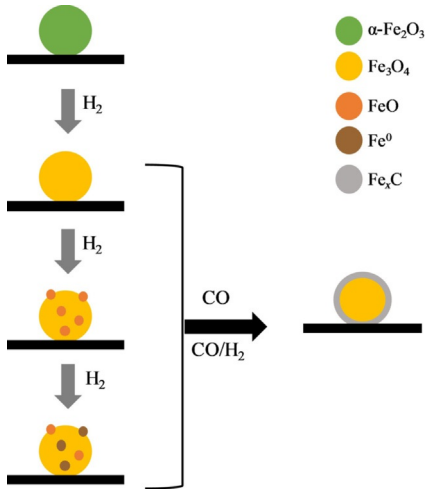

Scheme 3. Reduction and carburization steps of an iron-based catalyst.[83]

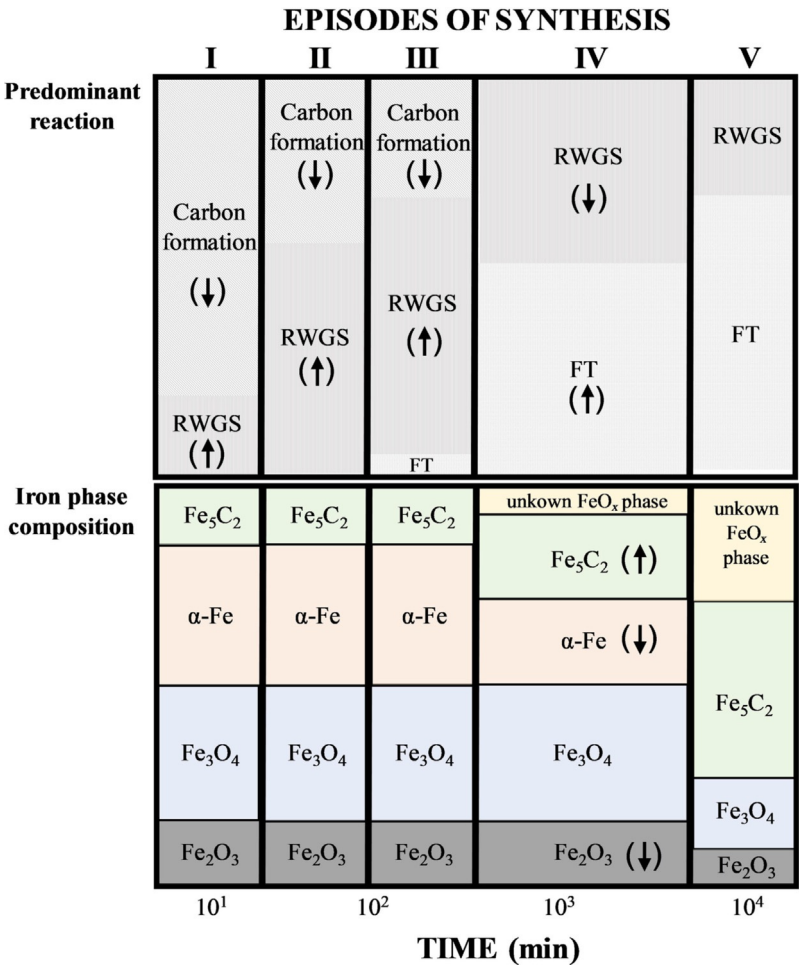

Scheme 4. Catalytic activity (top) and iron-phase composition of the catalyst (bottom) as a function of time during the reaction. Reaction conditions: $H_2/CO_2 = 3$, 250 °C, 1 MPa, Fe–Al–Cu–9 K catalyst. FT refers to the Fischer–Tropsch reaction. Arrows indicate the increase or decrease of reaction yield/iron phase during a certain episode.[84]

They identified five steps with different kinetic regimes, indicated as "episodes of synthesis". These steps were correlated to compositional and structural changes of the catalyst (Scheme 4). In episode I, the reactants adsorb onto the catalyst surface and carbon deposition takes place predominantly. This shows that the freshly reduced catalyst is not active in FTS. In episode II, carbon deposition continues and the products of RWGS are obtained. In episode III, RWGS activity increases, whereas carbon deposition declines. Between episodes I, II, and III, there is little change in the Fe-phase composition, but, in episode IV, if the FTS increases, metallic iron (α-Fe) is consumed and Fe_5C_2 carbide is formed. In episode V, FTS activity achieves steady state and all metallic iron is consumed. Even at steady-state conversion, the catalyst composition continues to change. Fe_2O_3 and Fe_3O_4 phases disappear and a new amorphous, probably oxidic, iron phase (FeO_x) forms. Because iron carbide is formed under a H_2/CO_2 atmosphere, freshly reduced catalysts usually show an induction period in CO_2 conversion upon exposure to the reactive feed.[69]

Several mechanisms for the FTS process were proposed. The most plausible route for the hydrocarbon formation reaction on iron-based catalysts is the carbide mechanism.[44] The monomer here is a methylene (CH_2) species. Scheme 5shows one of the proposed pathways, in which CO and H_2 adsorb dissociatively (1). Species such as CH, CH_2, and CH_3 can form this way (Scheme 5, pathway 2). Then, chain propagation occurs by insertion of the monomer into a growing alkyl chain (Scheme 5, pathway 3). Olefins are obtained if the process is terminated by dehydrogenation (Scheme 5, pathway 4). If, instead of dehydrogenation, a CH_3 species or hydrogen are added, paraffins will be obtained (Scheme 5, pathway 4).[44] Other pathways involving different surface species were also proposed. For example, in the enolic mechanism, undissociated adsorbed CO reacts with hydrogen. After that, the enolic monomer (HCHO) dissociates, giving water and methylene. Chain growth proceeds in a similar way to that in the carbide mechanism.[44] Mechanisms that involve different monomers were also described, involving CO insertion and formate and alkyl species.[35]

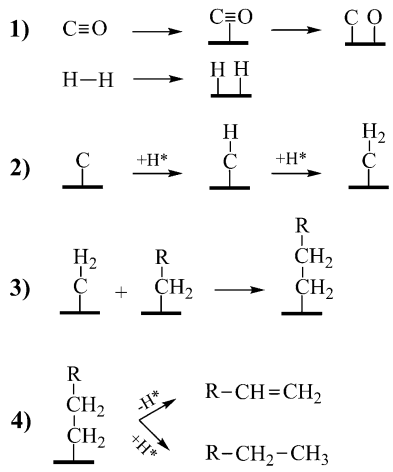

Scheme 5. Carbide mechanism for the FTS.[44]

These mechanisms correspond to the individual RWGS and FTS reactions. The overall CO_2 hydrogenation reaction mechanism was also proposed (Scheme 6).[36] First, CO_2 adsorbs on a Fe^{II} site (Scheme 6, step 1), which oxidizes the active site to Fe^{III}. Hydrogen dissociates on the formed surface group (Scheme 6, step 2). If the residual H• radical attacks the carbonyl C, formic acid is formed (Scheme 6, step 3b). If H• attacks the OH group, H_2O and CO are formed (Scheme 6, steps 3a and 4b). However, if the carbonyl radical formed after step 3a dissociates H_2 (Scheme 6, step 4a), the next H• can attack the group again and form either a formaldehyde (Scheme 6, step 5b) or an alcohol (from steps 5a to 7b). After Scheme 6, step 7a, the Fe–CH_2• radical is formed and is considered to be a carbon–carbon propagation species. The CH_2• radical attacks another CO_2 molecule and the reaction follows the same pathway. Termination occurs if hydrogen is abstracted from the carbon chain, which reduces the Fe species back and forms an olefin. Chain propagation is considered to be a major route because, in the performed study, the main products were higher hydrocarbons. The mechanism describes a redox pathway be-

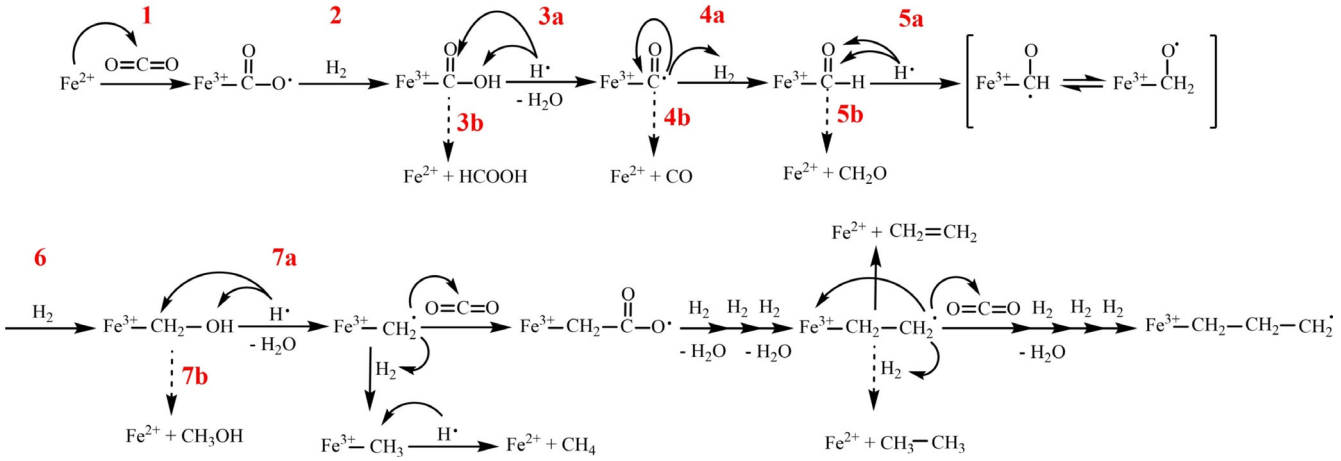

Scheme 6. Overall mechanism proposed for CO_2 hydrogenation to olefins.[36] Dashed arrows refer to the minor route and plain arrows to the major route.

tween iron active sites and CO_2, followed by chain propagation through a carbide-type mechanism.

Recent computational work indicated an alternative reaction pathway, without going through CO as intermediate if using Fe–Cu(100) surface, as shown in Equation (3).[57,85,86] The main path over a monometallic Fe (100) surface is shown in Equation (4).

$$CO_2^* \rightarrow HCOO^* \rightarrow HCOOH^* \rightarrow HCO^* \rightarrow HCOH^* \rightarrow CH \rightarrow CH{-}CH^* \quad (3)$$

$$CO_2^* \rightarrow CO^* \rightarrow HCO^* \rightarrow HCOH^* \rightarrow CH^* \rightarrow CH{-}CH^* \quad (4)$$

2.2. Catalytic CO_2 hydrogenation through the methanol-mediated route

2.2.1. The reaction

As shown in Scheme 1, the methanol-mediated synthesis of olefins comprises two reactions: CO_2 hydrogenation to methanol and methanol to olefins (MTO). The stoichiometric reaction of CO_2 hydrogenation to methanol is shown in Equation (5).

$$CO_2 + 3\,H_2 \rightleftharpoons CH_3OH + H_2O,\ \Delta H_{25\,^\circ C} = -49.5\,kJ\,mol^{-1} \quad (5)$$

Converting CO_2 into methanol is exothermic.[87] The endothermic RWGS reaction [Eq. (1)] occurs in parallel; thus CO is produced as a side product, especially at higher temperatures. The production of methanol in industry uses mixed syngas ($CO/H_2/CO_2$) as a feed and $Cu/ZnO/Al_2O_3$ as a commercial catalyst. The reaction runs at 210–270 °C and 50–100 bar (1 bar = 10^5 Pa).[88] This reaction is highly selective towards methanol (99%).[89] Methanol can be converted into olefins over a solid acid catalyst through the MTO reaction.[90] The involved reactions are shown in Equation (6). ZSM-5 and SAPO-34 are industrially used as catalysts for methanol conversion into olefins.[91] Further undesired recombination of olefins would produce paraffin, aromatics, and higher hydrocarbons.[92]

$$2\,CH_3OH \rightarrow CH_3OCH_3 + H_2O \rightarrow C_nH_{2n} + n\,H_2O \quad (6)$$

MTO is thermodynamically more favorable at high temperatures.[87] For instance, 400–450 °C is the optimal temperature over SAPO-34.[93] However, the previous step of the methanol-mediated route (CO_2 to methanol) is not favored at such high temperatures, and CO is produced instead through RWGS. Optimal CO_2 to methanol conversion was achieved at 300–325 °C.[94] The combination of both processes (CO_2 to methanol + MTO) requires a compromise in the reaction temperature, at which, ideally, CO formation is avoided ($\leq$300 °C), but the zeolite is active for C–C coupling ($\geq$350 °C).[95] Most recent publications on this topic run the reaction between 380 and 400 °C.

2.2.2. The catalysts

The catalysts used for CO_2 hydrogenation through the methanol-mediated route are usually composite materials comprising a methanol synthesis catalyst (mixed-metal oxides) and a zeolite for methanol conversion.[96] Excellent reviews on the advances in CO_2 hydrogenation to hydrocarbons, alkanes, and alcohols are available, covering the methanol-mediated route, among other strategies in the period until 2017.[37,97] Herein, we focus on recent reports on this topic (2017–2018). The metal oxide component of the bifunctional catalyst is responsible for CO_2 conversion to methanol and the zeolite component is responsible for further methanol conversion through selective C–C coupling.[98] Synergy between both phases decreases CO selectivity, thereby increasing olefin selectivity. The desired synergy is achieved if the components are in close contact.[87,98] Metal oxides and zeolites are usually incorporated together in the reactor; thus forming a physical mixture obtained by physical grinding (mortar-mixing method or shaking method).

There is no specific metal oxide for this bimetallic catalyst. The $Cu/ZnO/Al_2O_3$ system currently employed for methanol synthesis from mixed syngas exhibits limited activity in CO_2 hydrogenation, so it is not a good candidate. Previous work focuses on In_2O_3 and Ga_2O_3 metal oxides, in which the presence of oxygen vacancies plays a key role. These studies indicate that the oxygen vacancies of In_2O_3 and Ga_2O_3 may be the catalytic sites at which CO_2 is activated and hydrogenated to methanol.[93,99–101] ZrO_2 is sometimes added as a textural and electronic promoter. In CO_2 hydrogenation to olefins, adding ZrO_2 increases the stability of the catalyst by preventing sintering.[93,98] It also increases the density of oxygen vacancies, thereby increasing CO_2 activation.[98] These new oxygen vacancies can stabilize the key intermediates, decreasing the amount of the side product CO.[93,98] However, the presence of $>$40% CO in the product mixture is still a problem in this type of reaction.

The acid sites of zeolites are responsible for the chemical conversion of methanol into valuable hydrocarbons. Product selectivity is tuned by the zeolite pore architecture. ZSM-5 is one of the zeolites commonly used in methanol conversion reactions. It is an aluminosilicate with MFI topology of straight channels (5.1 × 5.4 Å) and intersecting sinusoidal channels (5.4 × 5.6 Å), forming a large space with a diameter of around 8.9 Å.[92,102] ZSM-5 has strong acid sites, which makes it active in methanol conversion. However, its large channels do not constrain the growth of hydrocarbons to form longer chain hydrocarbons and aromatics; thus lowering the selectivity to olefins. For this reason, it is typically used for the methanol to gasoline (MTG) process.[103] The structure of ZSM-5 can be tuned to obtain propylene in the methanol to propylene process (MTP).[104] Modifications include changing the Si/Al ratio, steam treatments, and inserting different metals.[105] Another popular catalyst for producing olefins is SAPO-34. This is a silicoaluminophosphate molecular sieve with the CHA framework that has large cages (6.7 × 10.9 Å) connected by smaller cavities (3.8 × 3.8 Å). The acid sites of SAPO-34 are weaker than those of ZSM-5, but SAPO-34 is more hydrothermally stable, and

therefore, more selective towards light olefins. For CO_2 hydrogenation, the structure of SAPO-34 is sometimes modified with zinc atoms to increase the basicity; thus restraining secondary reactions of the primary olefins.

Based on previous CO_2 to methanol catalysts, zinc-based bifunctional catalysts have been recently developed for CO_2 hydrogenation to olefins. Liu et al. showed that Cu–Zn–Al mixed oxide (the well-known catalyst for methanol synthesis from a mixture of CO, CO_2, and H_2) in combination with SAPO-34 provided only CO, paraffins, and methane as products, but not olefins.[95] The same researchers found that the combination of $ZnGa_2O_4$ mixed oxide with SAPO-34 could offer a high O/P ratio of 7.8. CO_2 conversion was 13%, with a relatively low CO selectivity (46%) and a high fraction of light olefins (86% calculated on a carbon basis, excluding CO). In another study, a "tandem" catalyst formed by ZnO–ZrO_2 mixed-metal oxide and Zn-doped SAPO-34 was tested.[87] The resulting catalyst (ZnZrO/SAPO) successfully converted 12.6% CO_2, with 47% CO selectivity. Among all hydrocarbon products, 80% were lower olefins ($C_2^=$–$C_4^=$), 14% C_2–C_4 paraffins, 3% CH_4, and 3% C_5^+ hydrocarbons. The catalytic behavior was maintained up to 100 h on stream without deactivation.

Regarding catalysts with ZrO_2, a bifunctional catalyst composed of indium–zirconium composite oxides and SAPO-34 zeolite was prepared.[93] The authors showed that the incorporation of Zr into In_2O_3 created new kinds of vacancies that enhanced the activity, relative to In_2O_3/SAPO-34 or ZrO_2/SAPO-34. On one hand, In_2O_3/SAPO-34 showed 32% CO_2 conversion and 86% CO selectivity and ZrO_2/SAPO-34 showed 9% CO_2 conversion and 97% CO selectivity. On the other hand, the In–Zr/SAPO-34 catalyst achieved 35.5% CO_2 conversion and 85% CO selectivity. Excluding CO, the selectivity to lower olefins was 72.4%, with a O/P ratio of 4.6. In addition, the incorporation of Zr increased the thermal stability of the catalyst. Dang et al. investigated the effect of the atomic ratio of In/Zr in the In_2O_3/ZrO_2/SAPO-34 catalyst.[98] The composite catalyst with a 4:1 atomic ratio of In/Zn showed the highest CO_2 conversion (26.2%); 74.5% lower olefins were obtained among the hydrocarbons, resulting in a O/P ratio of 3.5. DFT calculations in both studies suggested that CO_2 chemisorption at the oxygen vacancy sites near Zr atoms was much stronger, which stabilized the adsorption of intermediate species. This resulted in a decrease of RWGS activity and production of CO, which was beneficial for olefin formation. In a recent study, a core–shell CuZnZr@(Zn-)SAPO-34 catalyst was prepared and compared with a conventional, physically mixed composite.[106] The core–shell material showed higher CO_2 conversion and higher selectivity towards olefins, due to better control of the interface between the mixed oxide and SAPO-34, as well as the proximity of the two active sites.

The results obtained for catalysts of the methanol-mediated route are also shown in Table 2.

2.2.3. Reaction mechanisms

CO_2 hydrogenation to olefins by the methanol-mediated route is a coupling reaction of CO_2 to methanol and MTO. Experimental work shows that the catalyst needs to contain a combination of a metal oxide and a zeolite/molecular sieve.[87,93] Individual metal oxides can hydrogenate CO_2 to methanol, but they are not active for methanol conversion. Conversely, SAPO-34 alone is not active for CO_2 hydrogenation. Thus, the metal oxide component is responsible for CO_2 conversion to methanol and the zeolite component is responsible for further methanol conversion through selective C–C coupling. There is an agreement on where the reactions happen, but finding out how they take place remains a challenge.

Different reaction pathways were proposed for CO_2 hydrogenation to methanol, depending on the species formed if CO_2 is adsorbed and hydrogenated on the catalyst surface. Experimental and computational studies were used to identify the predominant intermediates during CO_2 hydrogenation on the Cu/ZrO_2 catalyst.[107] The results showed that carbonate and bicarbonate species formed if CO_2 adsorbed on the surface. Formate (HCOO) and methoxy (H_3CO) species were detected as reaction intermediates. A mechanistic study was performed on the Pd(111) surface during CO_2 hydrogenation to methanol by using DFT calculations.[108] The authors showed that CO_2 first hydrogenated to HCOO (formate intermediate) or COOH (carboxylic acid intermediate). They found that both routes could take place because the HCOO route had a lower activation barrier, but the COOH route was kinetically favorable. Both HCOO and COOH then reacted with surface H to form HCOOH, which next dissociated to HCO and OH. The hydrogenation of HCO species to form H_2CO, H_3CO, and finally H_3COH (route 1) was the most favorable route. A second route, through which HCO was hydrogenated to HCOH, had a higher activation barrier. Elsewhere, DFT calculations on the elementary Cu(111) surface showed that, after CO_2 hydrogenation, the stable intermediate was HCOO.[109] However, the authors proposed a different hydrogenation pathway through which HCHO was then hydrogenated to CH_3O_2. The splitting of the OH group formed CH_2O, which was hydrogenated to CH_3O to finally form CH_3OH. The overall hydrogenation sequence is $CO_2 \rightarrow HCOO \rightarrow HCOOH \rightarrow CH_3O_2 \rightarrow CH_2O \rightarrow CH_3O \rightarrow CH_3OH$. In summary, all studies agree that formates are key intermediates during CO_2 hydrogenation.

In situ IR spectroscopy on the $ZnGa_2O_4$ mixed oxide showed that carbonate species formed after the adsorption of CO_2.[95] The introduction of H_2 rapidly generated formates. Upon prolonging the reaction time, methoxide species became observable. Assuming that –Ga–O– and –Zn–O– pairs may dissociate H_2, generating H species, the overall hydrogenation of CO_2 was proposed in this study (Scheme 7). The formation of formates and methoxide species was also experimentally confirmed on the surfaces of the ZnZrO catalyst.[87] Scheme 7 shows the crucial role of oxygen vacancies in the catalytic cycle—they act as the active sites for CO_2 adsorption, based on the fact that the CO_2 conversion rate increases with an increase in the density of oxygen vacancies.

Many studies were performed on the MTO reaction. Nevertheless, C–C bond formation remains one of the most important questions in the MTO mechanism. Herein, we provide a summary of the most established mechanisms.[91,92] There are more than 20 proposed pathways for C–C bond generation

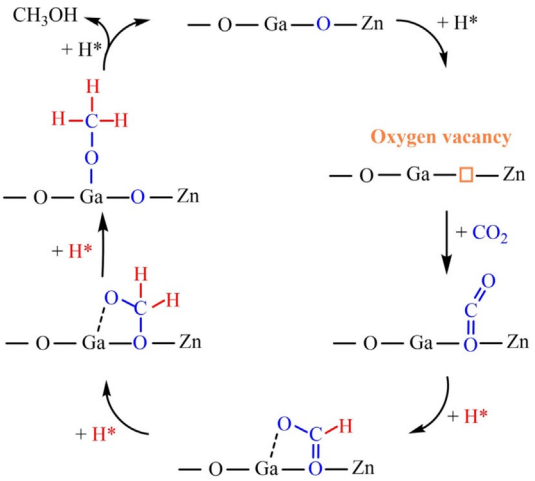

Scheme 7. Proposed reaction mechanism for the conversion of CO_2 to methanol over the Zn–Ga–O catalyst.[95]

from methanol, which are differentiated by the reaction intermediates. However, based on experimental evidence and theoretical calculations, reports in the literature acknowledge that this reaction follows an indirect mechanism. During MTO, the methanol conversion rate is very low in the initial stage, but it rises up to 100% suddenly after reacting for a period of time. This initial stage is the "dynamic induction period" and is difficult to explain by direct mechanisms. Once olefin products are initially formed, methanol conversion will increase through efficient indirect pathways with the regeneration of olefins or active cyclic organic compounds. Because the presence of small amounts of products leads to an enhanced rate of conversion, the MTO reaction is considered to be autocatalytic.

The pool mechanism is the most accepted indirect mechanism. It was proposed by Dahl and Kolboe at the beginning of the 1990s and is based on experimental data for SAPO-34.[110,112,113] Here, $(CH_2)_n$ represents the hydrocarbon pool, but the chemical structure of the pool was not completely specified. The authors proposed that methanol first formed active hydrocarbon pool species in the molecular sieve. Then, methanol reacts with the active hydrocarbon pool species to produce light olefins, and these olefins are further transformed by condensation, alkylation, cyclization, and hydrogen transfer to produce higher olefins, alkanes, and aromatic hydrocarbons (see Scheme 8a). Several changes and developments were proposed for the pool mechanism. The most accepted of these is the dual-based cycle concept, in which an aromatic-based cycle and an olefin-based cycle take place during the methanol to hydrocarbon reaction over ZSM-5.[111,114] In this cycle, ethane is formed from the methylation of lower methylbenzenes and side-chain elimination, whereas propene and higher alkenes form by alkene methylation and cracking. Propene can form through the aromatic-based cycle and, simultaneously, alkenes are converted into methylbenzenes through oligomerization and cyclization (Scheme 8b).

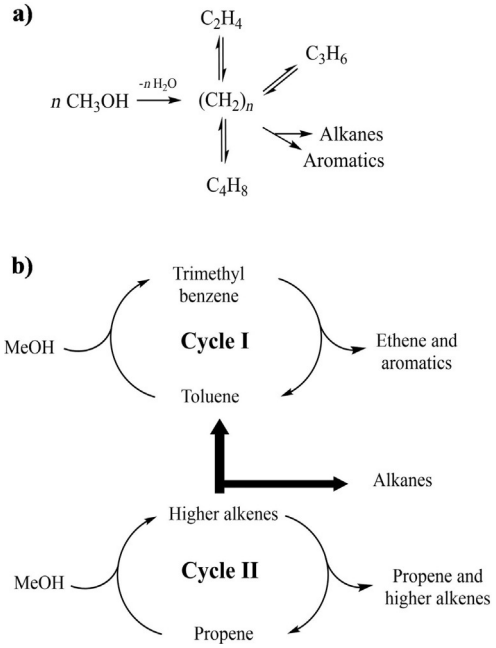

Scheme 8. a) Proposed hydrocarbon pool mechanism for the conversion of methanol over SAPO-34.[110] b) Proposed dual-cycle concept for the conversion of methanol over ZSM-5.[111]

2.3. Effects of operating conditions

Experimental conditions, such as temperature, pressure, H_2/CO_2 ratio, and space velocity, affect CO_2 conversion and the product distribution of the reaction. Taking the most recent publications on CO_2 hydrogenation, together with a reported thermodynamic analysis, we summarize herein the main effects of the experimental conditions on the reaction performance.

The effect of temperature on conversion and selectivity during CO_2 hydrogenation is not straightforward. Thermodynamic analysis by Yao et al. showed that reaction temperatures of around 400 °C were suitable for synthesizing light olefins.[45] At higher temperatures, RWGS is favored and CO selectivity increases.[87] Moreover, CO_2 conversion decreases at temperatures ranging from 100 to 450 °C.[45] However, experimental data does not show the same tendency. Iron-based catalysts (used in the MFTS route) or SAPO-34-based materials (methanol-mediated route) show higher CO_2 conversion upon increasing the temperature over the temperature range of 250–400 °C.[50,51,56,87,93,95] Optimal temperatures differ between studies, but a higher O/P ratio was obtained upon increasing the temperature from 200 to 300 °C.[51,56] A further increase of the temperature to 340 °C decreased the O/P ratio.[56]

Thermodynamic studies at 400 °C and a 3:1 H_2/CO_2 ratio showed that CO_2 conversion increased sharply if the pressure increased between 0 and 2 MPa.[45] At the same time, CO selectivity decreases with pressure. Above 2 MPa, the increase is less steep, but still between 3 and 5 MPa CO_2 conversion with an increase in olefin selectivity. Experimental data for a bulk Fe-based catalyst at 250 °C showed a strong increase in CO_2 conversion and a decrease in CO selectivity with pressures of up to 0.5 MPa, with minor improvements at 0.5–1 MPa.[50]

A SAPO-34 catalyst at 380 °C showed the same tendency, but with fewer olefins and more paraffins in the hydrocarbon distribution upon increasing pressure from 1 to 5 MPa.[93]

The effect of the H_2/CO_2 molar ratio on the thermodynamic equilibrium conversion (400 °C, 3 MPa) shows an increase in CO_2 conversion upon increasing the H_2/CO_2 ratio.[45] In addition, selectivity towards C_{2-5} olefins is predominant if the H_2/CO_2 ratio is higher than three. Experiments with bulk Fe_2O_3 catalysts (MFTS route) showed an increase in CO_2 conversion, a decrease in CO selectivity, and an increase in CH_4 selectivity upon increasing the H_2/CO_2 molar ratio from 1 to 3 MPa.[50] The rate of CO hydrogenation to hydrocarbons increases with increasing H_2 content and the O/P ratio is slightly lower at 3 MPa due to further hydrogenation of olefins. Catalysts for the methanol-mediated route for CO_2 hydrogenation show similar results.[93]

Regarding the effect of adding an inert gas, upon increasing the N_2/CO_2 ratio, the CO_2 conversion and total olefin selectivity decrease by around 10%.[45] Conversely, propene selectivity rises at the same time. Adding N_2 has little influence on the conversion of CO_2, but is beneficial to the selectivity of propene. In addition, because in the MFTS route all reactions are exothermic, the addition of an inert gas will help to dissipate heat generated by the process.

Experimental studies have determined the effect of the space velocity, which is expressed as $mL\,g_{cat.}^{-1}\,h^{-1}$. Higher space velocities decrease CO_2 conversion values due to the reduced contact time. In most cases, C_2–C_4 olefin selectivity is increased with the space velocity because there is not enough time to convert olefins into higher olefins, alkanes, or CH_4,[87,93] although there are some exceptions.[50]

2.4. Catalyst deactivation and its causes

Both MFTS and methanol-mediated CO_2 hydrogenation routes give water as a byproduct. This water can be a problem for the reaction equilibrium and catalyst stability. High concentrations of water vapor in the gas mixture decrease the CO_2 conversion rate because the equilibrium is limited.[45] A high water partial pressure can also affect the catalyst by enhancing oxidation or sintering of the active sites.[115,116] Although this issue was studied in the FTS reaction,[117] MFTS CO_2 hydrogenation studies rarely refer to the effect of water on the catalytic performance. This might be because the latest studies always introduce potassium as a promoter, which has been shown to enhance the resistance of the catalyst towards oxidation.[118] The incapability of the catalyst (in both routes) to achieve higher conversion values may reflect the production of water as a side product. To remove water during the reaction, one of the best solutions is to use inorganic water permeoselective membranes.[119,120] Common deactivation problems, such as coking and thermal sintering, were reported for iron-based catalysts during MFTS CO_2 hydrogenation.[77,121] Phase changes during the reaction can also lead to a decrease in conversion. Further carbidization of χ-Fe_5C_2 gives θ-Fe_3C, which is not active in FTS.[49]

Regarding the effect of water on methanol-mediated CO_2 hydrogenation, water can also affect the acid sites of the zeolites. Hydrophobic modifications of zeolites with organic compounds were performed to improve their stability in water.[96] Steam treatments were also applied to decrease deactivation.[105] In addition, SAPO-34 (the most common zeolite used in CO_2 hydrogenation to olefin catalysts) has a high hydrothermal stability, which prevents its deactivation. Zeolites can also suffer from coking because the acid sites enhance the formation of carbon deposits.[98] SAPO-34 suffers more from coking than ZSM-5 because of its smaller pore size. Increasing the mesoporosity of SAPO-34 while preserving the micropores, can decrease the rate of deactivation.[105] Another approach is to decrease the crystallite size through microwave synthesis.[122] Agglomeration of metal oxide nanoparticles in a SAPO-34 catalyst was also observed to be a factor for deactivation at 400 °C.[93] This problem can be prevented, for example, by adding ZrO_2 to the metal phase.

2.5. Implementation of CO_2 hydrogenation in industry

To date, CO_2 hydrogenation to olefins is performed on the laboratory scale only. The need for a better catalyst to improve the reaction efficiency is slowing its commercialization. However, another important issue is the technology to obtain the main reagents: hydrogen and carbon dioxide. In this section, we discuss the current status of the production of renewable H_2 and capture of CO_2. Regarding the economics of these processes, the main bottlenecks are the price of renewable energy for the production of renewable H_2, and the capture and transport of CO_2.

In the production of hydrogen, the total cost and carbon footprint of the process are influenced by technology. H_2 is currently commercially obtained from steam methane reforming (SMR). SMR requires (natural) gas as a feedstock and emits CO_2,[123] which does not help the environmental problem we are addressing. Electrolysis is the main alternative for the production of H_2, if renewable energy is used in the process. Renewable energy is mainly obtained from wind power, hydropower, and solar photovoltaics, or from an excess of electrical energy obtained from non-carbon-based sources (nuclear power plants during the night).[124,125] One of the main drawbacks of using renewable energy is its storage because the demand for electricity is not constant over time. Although the storage of this energy in batteries or electric grids is under development, the production of H_2 with a surplus of energy from renewable electric plants will help to alleviate the storage problem. Renewable energy is then used to produce renewable H_2 through water electrolysis [Eq. (7)].

$$2\,H_2O \rightarrow 2\,H_2 + O_2,\ \Delta H_{STP} = 237\,kJ\,mol^{-1} \qquad (7)$$

Water electrolysis is a strongly endothermic process. Even at 100% efficiency, it requires nearly 40 kWh to produce 1 kg of hydrogen.[126] There are various types of electrolyzers. Alkaline electrolysis (alkaline electrolysis cell) is the oldest technology. It is generally cheap due to the low cost of the electrode materi-

als (usually nickel), but its efficiency is limited.[127,128] The proton exchange membrane (PEM) is younger technology that shows higher efficiencies.[129] It presents several advantages, such as high response rate and production of H_2 under pressure, in modern electrolyzers; thus avoiding further compression steps.[125] However, many of the PEM electrolyzers use IrO_2 as their anode catalyst, which increases the capex.[130] Solid oxide electrolysis cells operate at a high temperature (950–1000 °C), which results in higher efficiencies; this technology is still in development.[131,132]

The main bottlenecks to establishing electrolysis as a preferred technology to produce H_2 are the price of crude oil and the price of renewable energy, that is, competition between old and new technologies. The price of renewable H_2 mainly depends on the cost of renewable electricity and the cost of electrolysis technology. Previous reports estimate that 1 kg of renewable H_2 will cost around €8–10 by 2020.[125] This is still too expensive for industrial implementation. In addition, an electrolysis plant nowadays is much smaller in capacity than that of a SMR plant. There are, however, efforts for rapid scaling of technology. Several companies are already developing electrolysis plants. Siemens is a large producer: it supplied 6 MW, by using PEM electrolyzers, to the power-to-gas project Energiepark Mainz in 2014.[133] The installation of PEM electrolyzers keeps expanding: in 2018, Air Liquide installed HyBalance; a pilot site for the production of carbon-free hydrogen.[134] The electrolyzer, with a capacity of 1.2 MW, produces about 500 kg hydrogen per day.

The second reactant we need is CO_2. CO_2 emissions come mainly from power plants and heavy-industry flue gases. Technologies for capturing CO_2 directly at the emission source are being developed.[8] However, the further implementation of these technologies will only take place if it is economically profitable for industry. The cost of CO_2 (or tax on its emission) needs to be significant enough for companies to reconsider discarding it. In November 2017, the price of a tonne of CO_2 under the European Union Emissions Trading Scheme (EU ETS) was approximately €8.[126] The EU ETS price is expected to increase, but stricter measures are needed. If coming from flue gases, the source of CO_2 will determine its purity and the cost-efficiency of its recovery. High-purity CO_2 can be obtained from chemical processes such as ammonia production, ethylene oxide production, and H_2 production from natural gas.[135] During the production of bioethanol or biomethane in biorefineries, a considerable amount of CO_2 is produced and usually released into the atmosphere.[136]

Several companies, including the Linde Group and Air Liquide, are already investing in CO_2 capture. The Linde Group is focused on developing and improving technologies for coal-fired power stations.[137] Air Liquide has developed a CO_2 capture technology based on a cryogenic process (Cryocap) that can be adapted to specific applications: steel plants, thermal power stations, or hydrogen production units.[138] In 2015, a Cryocap unit was connected to Air Liquide's largest hydrogen production unit in France, with an annual capture capacity of 100 000 tons of CO_2. Each industrial process will require a tailor-made solution for CO_2 recovery. CO_2 capture technologies are commonly classified as precombustion capture, postcombustion capture, and oxyfuel combustion capture.[139] Large-scale postcombustion capture systems are already operational. They are mainly based on liquid amine adsorption techniques. A technoeconomic study on CO_2 chemisorption in MEA is reported elsewhere.[126] Based on the literature,[140] the authors estimated a capital cost of adsorption of about €80 per tonne of CO_2 capture capacity per year for a capture plant with a lifetime of 20 years delivering 99.9% pure CO_2 at 99.9% yield. Electricity consumption is 55 kWh t^{-1} CO_2 for the capture process and 115 kWh t^{-1} CO_2 for compressions to 110 bar (needed for transportation). To regenerate the MEA solvent, a low-pressure steam consumption of 3.2 GJ t^{-1} CO_2 is needed.[141] The overall cost comes to €35 t^{-1} CO_2. Different studies approximate €60 t^{-1} CO_2 or €25 t^{-1} CO_2 if waste heat can be used.[142]

Another important possibility is direct air capture (DAC). This process is mainly limited by the low CO_2 concentration in the atmosphere (400 ppm).[143] DAC technologies use chemical sorbent materials. If the sorbent is full, heat is used to release CO_2 molecules in a very pure stream. The processes differ in design and sorbent. DAC is a relatively young technology and its capture costs are estimated at €40 t^{-1} CO_2.[126,144]

Even after capture, CO_2 compression and transport remain expensive. Trucks are commonly used to deliver CO_2 by road. The transportation costs will depend on the delivery distance and size of the tanker. It was estimated that in a biomethane production plant the price of only transportation was €25–40 t^{-1} CO_2.[136] In addition, if the transport of CO_2 is achieved by using fossil-fuel-based trucks, this will emit further CO_2 into the atmosphere. Transport of CO_2 by pipelines is also being studied, but this is only cheaper than that of transport by truck on a large scale.[139] Pipelines are already operational, for example, the CO_2 Smart Grid is a climate initiative that plans a large-scale CO_2 transportation infrastructure across the Netherlands.[145] The CO_2 Smart Grid plan is based on the existing CO_2 pipeline infrastructure in the Netherlands (operated by OCAP), potential CO_2 suppliers, potential geological storage locations, current CO_2 demand by the horticultural industry, and future CO_2 demand for innovative reuse technologies. The current OCAP infrastructure delivers approximately 450 kilotons of CO_2 to around 500 greenhouses annually. Shell's Pernis refinery and the Alco biorefinery are already connected to the OCAP network for CO_2 delivery.

2.6. Discussion

The two CO_2 hydrogenation routes are differentiated by the type of catalyst. In Scheme 9, we show an overview of the most commonly used catalysts for CO_2 hydrogenation. In the MFTS route, iron catalysts are preferred (usually doped with alkali metals). Alkali metals, especially potassium, are essential as promoters for obtaining high selectivity to olefins. γ-Al_2O_3 is the most commonly used support. Nontraditional supports, such as MOFs and porous carbons, are less stable and give lower olefin yields. The conversion of these catalysts can be increased by adding metals, such as Cu, Co, Mn, or Zn. Converse-

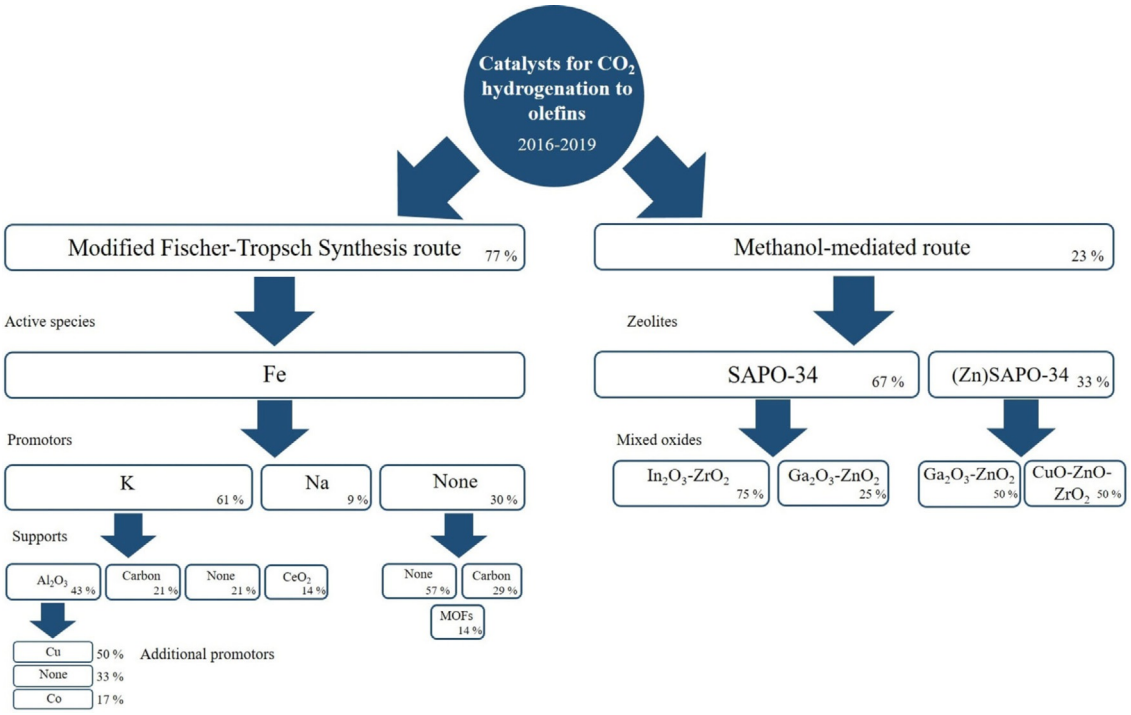

Scheme 9. Catalysts for CO_2 hydrogenation to olefins. The percentages are calculated based on 26 papers published between 2016 and the beginning of 2019.

ly, the methanol-mediated route is catalyzed by Group IIIA metal oxides, such as In_2O_3 and Ga_2O_3. ZrO_2 is added to increase the number of vacancies and the overall stability. SAPO-34 is an essential part of the bifunctional catalyst for olefin synthesis.

The MFTS route has better catalytic performance than that of the methanol-mediated route. At the same CO_2 conversion level (see Table 2), it gives higher selectivity to olefins, but the MFTS route also has a theoretical limit for C_2–C_4 olefin selectivity because it follows the ASF distribution for which the maximum yield of C_2–C_4 olefins is about 60%.[34] The methanol-mediated route does not have this limitation. Light olefin selectivity values (excluding CO) were reported to be up to 80%.[93] However, this holds only at low CO_2 conversion (≈13%). Higher conversion will result in more side reactions and lower olefin selectivity.

Overall, the main challenge of CO_2 hydrogenation is the wide product distribution, which is independent of the route. Apart from CO and CH_4, C_2–C_4 alkanes and C_{5+} hydrocarbons are present; these hinder industrial application. These findings are in line with previous reviews,[31,32,36,37,40,97] which emphasize the need for a better understanding of the reaction pathways and structure–activity correlations. To enhance catalysis, we believe that the following four aspects should be focused upon:

1) Increase the C/H ratio on the catalyst surface if following the MFTS route. First, increasing the amount of adsorbed CO_2 with an optimum bond strength is beneficial for CO_2 conversion. Second, once olefins are formed, readsorption and further reaction lead to the formation of side products, such as alkanes, through hydrogenation. Increasing the metal–C bond strength, compared with the metal–H bond, would increase the C/H ratio, which, in turn, would inhibit the readsorption of olefins and secondary reactions. This aspect has been addressed by doping iron-based catalysts with alkali metals, commonly potassium. Alkali metals have been shown to accelerate alkene desorption from the surface and suppress secondary hydrogenation of alkenes.[60] The addition of these dopants is a key factor that makes catalysts more suitable for the production of olefins, rather than paraffins. However, as observed from the results in Table 2, the olefin selectivity is still low. The development of new and efficient synthetic methods would increase olefin selectivity. For example, K in a K-doped Fe/C catalyst derived from biopromoters (combustion of corncob) showed stronger migration ability than that of K in chemical promoters during CO_2 hydrogenation.[20] This effect leads to a potassium-enriched surface that could promote the formation of carbides and suppress alkene hydrogenation; thus resulting in a higher amount of olefins.
2) In the methanol-mediated route, the interface and proximity of the two catalyst components affect the product distribution. Close proximity and a large interface between oxides and SAPO-34 reduce the acidity of the latter, which decreases secondary hydrogenation reactions, and therefore, increases olefin selectivity. To date, physical mixing is the preferred technique, but other synthetic methods should be explored. Recent studies already showed the benefits of using core–shell catalysts versus those that are physically mixed.[106]
3) The mechanism of CO_2 hydrogenation remains unclear. The reaction pathways of either MFTS or the methanol-mediat-

ed route are based on individual reactions. In situ characterization and computational studies are needed to gain an insight into the overall mechanism and improve the catalyst design process.

4) Regarding the catalyst stability, it is important to understand the effect of water as a side product. We believe that the removal of water during the reaction would increase conversion and the catalyst stability.

Regarding the third point, the fact that CO_2 hydrogenation is a two-step reaction makes it difficult to study the overall mechanism. To date, the general approach has been to study the mechanism by looking at individual reactions.

On one hand, knowledge of CO_2 hydrogenation through the MFTS route is based on the two reactions that take place: the RWGS reaction on iron-based catalysts and the C–C coupling reaction based on FTS studies. The latest studies in this field make use of computational calculations (DFT) to elucidate the reaction pathway on Fe and Fe–Cu catalysts.[85,86] The authors proposed formates as reaction intermediates if a Fe–Cu catalyst was used. On the other hand, Satthawong et al. concluded that CO was the reaction intermediate with a Fe–Co catalyst.[68] The authors based their findings on detecting variations in the product distribution upon changing the reaction parameters. There are no spectroscopic studies that confirm the formation of formates or CO as reaction intermediates. Therefore, for the MFTS route, one needs to combine spectroscopic techniques (under conditions similar to those employed during the reaction) with kinetic and computational studies to confirm which species are the reaction intermediates. This will depend on the catalyst and reaction conditions used.

Recent studies on the methanol-mediated route used ex situ and in situ spectroscopy and DFT calculations to elucidate the reaction intermediates.[87,93,95,98] An excellent example is the study of CO_2 hydrogenation on a Cu/ZrO_2 catalyst performed by Larmier et al.[107] Using kinetic studies, in situ diffuse reflectance infrared Fourier transform spectroscopy (DRIFTS), and NMR spectroscopy combined with isotopic labeling strategies, as well as DFT, they showed that formate and methoxy species were formed during the reaction. Similar conclusions were obtained by Li et al.,[87] who used in situ DRIFTS and quantitative analysis through a chemical trapping–mass spectrometry method. Nevertheless, these studies limit their mechanistic investigations into CO_2 to methanol conversion, with no in-depth studies on the MTO reaction.

Studying the two steps individually makes sense. However, we cannot conclude that the overall reaction will follow an identical pathway if a bifunctional catalyst is used. Studying the overall mechanism remains a challenge due to the complex reaction network. As indicated by Ma and Porosoff,[40] more realistic DFT calculations (not only over single crystals, but over heterogeneous catalysts ensembles, as well as under real reaction conditions) together with spectroscopic analysis will make an impact on knowledge of the reaction pathway. The catalyst design also will benefit from the application of multiscale modeling combining different reactor length scales, including the catalyst active center, adsorption, and diffusion processes inside the pores and full-scale reactor.[147] The coupling of first-principles with computational fluid dynamics and reactor-scale simulations can translate molecular-scale mechanistic knowledge to the reactor scale; thus enabling comparisons with in situ and in operando experimental measurements. An example is the recent report on the simulation of CO oxidation on RuO_2 at the reactor scale, which was compared with experimental studies employing catalytic powders consisting of microscale particles.[148] Such studies are scarce and need to be carried out.

Wide product distribution problems can be tackled by using the different diffusion abilities of olefins and paraffins in a porous structure, as well as their affinity to metal sites, to manipulate the yield of the desired products. For example, in a mixture of olefins and paraffins, siliceous zeolites often give high selectivity to olefins. In contrast, cationic zeolites and titanosilicates preferentially adsorb olefins. Recently, it was reported that a pure silica zeolite could kinetically separate ethylene from ethane with a high selectivity, by utilizing its distinctive pore topology and framework flexibility.[149] Another example is the use of zeolites with DDR topology in the MTO reaction. High selectivity towards light olefins was obtained by using this topology. The formation of hydrocarbons bigger than C_4 was suppressed completely and only traces of ethane and propane were formed. In addition, the selective removal of silanol defects by a mild treatment in the presence of NaOH/cetyltrimethylammonium bromide improved the catalyst lifetime.[146] Thus, the identification of suitable topologies of porous materials and understanding the physicochemical properties that influence the diffusion and adsorption of olefins and paraffins within the structural framework, whether it is neutral or charged, can help significantly in designing new catalysts for CO_2 to olefin conversion.

Because most of the studies published in 2018 focused on the development of catalysts for the methanol-mediated route, we expect increasing interest and a faster development of catalysts for this type of reaction. In addition, the two reactions that take place in the process (CO_2 to methanol and the MTO reaction) are commercialized individually, so the implementation of a process that incorporates both steps might be easier than that for the MFTS route. Research should focus on developing materials with a strategic placement of different functionalities and on improving the interfacial contact of the catalyst. We believe that these factors will improve the reaction performance; thus bringing CO_2 hydrogenation closer to industrial application.

3. Summary and Outlook

The two main routes for catalytic CO_2 hydrogenation to olefins are the MFTS route and the modified-methanol route. In both cases, avoiding the formation of side products, such as CO, CH_4, C_2–C_4 alkanes, and C_{5+} hydrocarbons, is crucial for industrial implementation. This needs further research efforts, such as modifications of the relative strengths of metal–carbon and metal–H bonds, strategic placement of different functions within the catalyst, and an understanding of the mechanism of

the combined reaction. In addition to catalyst design and product distribution, other challenges must be met before these reactions can be applied on a large scale. First, renewable H_2 production is under development, and several electrolyzers have been commercialized; however, electrolysis is still too costly. CO_2 compression and transport remain an issue, due to high costs and emission of GHGs. Although the cost of renewable H_2 will strongly depend on the price of renewable energy, estimations shown herein indicate that the production of H_2 from PEM electrolyzers is more expensive than that of the capture and transport of CO_2 from flue gases. Thus, the use of CO_2 and H_2 as clean olefin sources remains a challenge. Economic and social incentives can encourage investigations that aim to develop more efficient catalysts, as well as attempts to make the production of renewable H_2 and capture of CO_2 more economically attractive.

Acknowledgements

We thank the Netherlands Scientific Organisation (NWO) for the grant "Developing novel catalytic materials for converting CO_2, methane and ethane to high-value chemicals in a hybrid plasma-catalytic reactor" (China.15.119), and Dr. David Dubbeldam (University of Amsterdam) for discussions on the computational chemistry part.

Conflict of interest

The authors declare no conflict of interest.

Keywords: heterogeneous catalysis · hydrogenation · olefins · renewable resources · synthesis design

[1] D. Lüthi, M. Le Floch, B. Bereiter, T. Blunier, J. M. Barnola, U. Siegenthaler, D. Raynaud, J. Jouzel, H. Fischer, K. Kawamura, T. F. Stocker, *Nature* **2008**, *453*, 379 – 382.
[2] S. C. Peter, *ACS Energy Lett.* **2018**, *3*, 1557 – 1561.
[3] Shell International B.V., *Shell Scenarios. Sky. Meeting the goals of The Paris agreement*, can be found under https://www.shell.com/promos/business-customers-promos/download-latest-scenario-sky/_jcr_content.stream/1530643931055/eca19f7fc0d20adbe830d3b0b27bc-c9ef72198f5/shell-scenario-sky.pdf (accessed June **2018**).
[4] Shell International B.V., *Shell Scenarios. The Numbers behind Sky.*, https://www.shell.com/promos/business-customers-promos/numbers-behind-sky/_jcr_content.stream/1530643757647/c6da-f2e0c93fd3d724f2804837d053fdd24e0553/shell-sky-scenario-data-2018.xlsx (accessed June **2018**).
[5] A. Das, L. Emele, F. Meinke-Hubeny, I. Moorkens, C. Nissen, M. Tomescu, European Enviornmental Agency (EEA), *Renewable Energy in Europe-2018: Recent Growth and Knock-on Effects*, **2018**, http://www.eea.europa.eu/publications/renewable-energy-in-europe-2018 (accessed April **2019**).
[6] D. Gielen, L. Janeiro, L. Gutierrez, G. Prakash, D. Saygin, International Renewable Energy Agency (IRENA), *Renewable Energy Prospects for the European Union*, **2018**, http://www.irena.org/publications/2018/Feb/Renewable-energy-prospects-for-the-EU (accessed April **2019**).
[7] R. Ferroukhi, D. Nagpal, D. Hawila, M. Renner, B. Parajuli, B. Franceschini, S. Lozo, J. J. Lee, C. Strinati, T. Rinke, M. Taylor, A. Ilas, J. Estima, A. O. Ali, A. Khalid, J. Curtis, T. Raassina, International Renewable Energy Agency (IRENA), *Renewable Energy Market Analysis: Southeast Asia*, **2018**, http://www.irena.org/publications/2018/Jan/Renewable-Energy-Market-Analysis-Southeast-Asia (accessed April **2019**).
[8] R. M. Cuéllar-Franca, A. Azapagic, *J. CO2 Util.* **2015**, *9*, 82 – 102.
[9] A. Kothandaraman, L. Nord, O. Bolland, H. J. Herzog, G. J. McRae, *Energy Procedia* **2009**, *1*, 1373 – 1380.
[10] A. J. Hunt, E. H. K. Sin, R. Marriott, J. H. Clark, *ChemSusChem* **2010**, *3*, 306 – 322.
[11] T. Sakakura, J. C. Choi, H. Yasuda, *Chem. Rev.* **2007**, *107*, 2365 – 2387.
[12] M. Behrens, *Angew. Chem. Int. Ed.* **2016**, *55*, 14906 – 14908; *Angew. Chem.* **2016**, *128*, 15128 – 15130.
[13] *Carbon Recycling International*, can be found under http://www.carbonrecycling.is/george-olah (accessed January **2019**).
[14] O. S. Bushuyev, P. De Luna, C. T. Dinh, L. Tao, G. Saur, J. van de Lagemaat, S. O. Kelley, E. H. Sargent, *Joule* **2018**, *2*, 825 – 832.
[15] Y. Zheng, W. Zhang, Y. Li, J. Chen, B. Yu, J. Wang, L. Zhang, J. Zhang, *Nano Energy* **2017**, *40*, 512 – 539.
[16] B. Ashford, X. Tu, *Curr. Opin. Green Sustainable Chem.* **2017**, *3*, 45 – 49.
[17] X. Ma, S. Li, M. Ronda-Lloret, R. Chaudhary, L. Lin, G. van Rooij, F. Gallucci, G. Rothenberg, N. R. Shiju, V. Hessel, *Plasma Chem. Plasma Process.* **2019**, *39*, 109 – 124.
[18] D. Zhang, Q. Huang, E. J. Devid, E. Schuler, N. R. Shiju, G. Rothenberg, G. Van Rooij, R. Yang, K. Liu, A. W. Kleyn, *J. Phys. Chem. C* **2018**, *122*, 19338 – 19347.
[19] P. W. N. M. van Leeuwen, *Homogeneous Catalysis*, Springer, Dordrecht, **2004**, pp. 175 – 190, Chap. 9.
[20] L. Guo, J. Sun, X. Ji, J. Wei, Z. Wen, R. Yao, H. Xu, Q. Ge, *Chem. Commun.* **2018**, *1*, 11.
[21] H. M. T. Galvis, K. P. de Jong, *ACS Catal.* **2013**, *3*, 2130 – 2149.
[22] F. Cavani, F. Trifirò, *Appl. Catal. A* **1992**, *88*, 115 – 135.
[23] N. Madaan, R. Haufe, N. R. Shiju, G. Rothenberg, *Top. Catal.* **2014**, *57*, 1400 – 1406.
[24] *Handbook of Heterogeneous Catalysis, Vol. 6*, Section 13.4 (Eds.: G. Ertl, H. Knözinger, F. Schüt, J. Weitkamp), Wiley-VCH, Weinheim, **2008**.
[25] A. Corma, F. V. Melo, L. Sauvanaud, F. Ortega, *Catal. Today* **2005**, *107 – 108*, 699 – 706.
[26] World Economic Forum, Ellen MacArthur Foundation and McKinsey & Company, *The New Plastics Economy—Rethinking the Future of Plastics*, **2016**, http://www.ellenmacarthurfoundation.org/publications/the-new-plastics-economy-rethinking-the-future-of-plastics (accessed December **2018**).
[27] T. Ren, M. Patel, K. Blok, *Energy* **2006**, *31*, 425 – 451.
[28] T. Ren, M. K. Patel, K. Blok, *Energy* **2008**, *33*, 817 – 833.
[29] R. Faiz, K. Li, *Chem. Eng. Sci.* **2012**, *73*, 261 – 284.
[30] M. Azhin, T. Kaghazchi, M. Rahmani, *J. Ind. Eng. Chem.* **2008**, *14*, 622 – 638.
[31] A. V. Puga, *Catal. Sci. Technol.* **2018**, *8*, 5681 – 5707.
[32] S. Saeidi, N. A. S. Amin, M. R. Rahimpour, *J. CO2 Util.* **2014**, *5*, 66 – 81.
[33] W. Wang, S. Wang, X. Ma, J. Gong, *Chem. Soc. Rev.* **2011**, *40*, 3703 – 3727.
[34] R. W. Dorner, D. R. Hardy, F. W. Williams, H. D. Willauer, *Energy Environ. Sci.* **2010**, *3*, 884 – 890.
[35] S. Saeidi, S. Najari, F. Fazlollahi, M. K. Nikoo, F. Sefidkon, J. J. Klemeš, L. L. Baxter, *Renewable Sustainable Energy Rev.* **2017**, *80*, 1292 – 1311.
[36] H. Yang, C. Zhang, P. Gao, H. Wang, X. Li, L. Zhong, W. Wei, Y. Sun, *Catal. Sci. Technol.* **2017**, *7*, 4580 – 4598.
[37] W. Li, H. Wang, X. Jiang, J. Zhu, Z. Liu, X. Guo, C. Song, *RSC Adv.* **2018**, *8*, 7651 – 7669.
[38] G. Prieto, *ChemSusChem* **2017**, *10*, 1056 – 1070.
[39] L. Guo, J. Sun, Q. Ge, N. Tsubaki, *J. Mater. Chem. A* **2018**, *6*, 23244 – 23262.
[40] Z. Ma, M. D. Porosoff, *ACS Catal.* **2019**, *9*, 2639 – 2656.
[41] Q. Wang, Y. Chen, Z. Li, *J. Nanosci. Nanotechnol.* **2019**, *19*, 3162 – 3172.
[42] T. Riedel, G. Schaub, K.-W. Jun, K.-W. Lee, *Ind. Eng. Chem. Res.* **2001**, *40*, 1355 – 1363.
[43] J. Wei, Q. Ge, R. Yao, Z. Wen, C. Fang, L. Guo, H. Xu, J. Sun, *Nat. Commun.* **2017**, *8*, 15174 .
[44] G. P. van der Laan, A. A. C. M. Beenackers, *Catal. Rev. Sci. Eng.* **1999**, *41*, 255 – 318.
[45] B. Yao, W. Ma, S. Gonzalez-Cortes, T. Xiao, P. P. Edwards, *Greenhouse Gases: Sci. Technol.* **2017**, *7*, 942 – 957.
[46] R. Dorner, D. Hardy, F. Williams, *Energy Fuels* **2009**, *23*, 4190 – 4195.

[47] E. de Smit, B. M. Weckhuysen, *Chem. Soc. Rev.* **2008**, *37*, 2758 – 2781.
[48] M. Zhu, I. E. Wachs, *ACS Catal.* **2016**, *6*, 722 – 732.
[49] E. de Smit, F. Cinquini, A. M. Beale, O. V. Safonova, W. van Beek, P. Sautet, B. M. Weckhuysen, *J. Am. Chem. Soc.* **2010**, *132*, 14928 – 14941.
[50] C. G. Visconti, M. Martinelli, L. Falbo, A. Infantes-Molina, L. Lietti, P. Forzatti, G. Iaquaniello, E. Palo, B. Picutti, F. Brignoli, *Appl. Catal. B* **2017**, *200*, 530 – 542.
[51] M. Albrecht, U. Rodemerck, M. Schneider, M. Bröring, D. Baabe, E. V. Kondratenko, *Appl. Catal. B* **2017**, *204*, 119 – 126.
[52] T. Wu, J. Lin, Y. Cheng, J. Tian, S. Wang, S. Xie, Y. Pei, S. Yan, M. Qiao, H. Xu, B. Zong, *ACS Appl. Mater. Interfaces* **2018**, *10*, 23439 – 23443.
[53] J. Wang, Z. You, Q. Zhang, W. Deng, Y. Wang, *Catal. Today* **2013**, *215*, 186 – 193.
[54] M. C. Ribeiro, G. Jacobs, B. H. Davis, D. C. Cronauer, A. J. Kropf, C. L. Marshall, *J. Phys. Chem. C* **2010**, *114*, 7895 – 7903.
[55] P. A. Chernavskii, V. O. Kazak, G. V. Pankina, Y. D. Perfiliev, T. Li, M. Virginie, A. Y. Khodakov, *Catal. Sci. Technol.* **2017**, *7*, 2325 – 2334.
[56] M. Bradley, R. Ananth, H. Willauer, J. Baldwin, D. Hardy, F. Williams, *Molecules* **2017**, *22*, 1579.
[57] W. Wang, X. Jiang, X. Wang, C. Song, *Ind. Eng. Chem. Res.* **2018**, *57*, 4535 – 4542.
[58] S. Li, A. Li, S. Krishnamoorthy, E. Iglesia, *Catal. Lett.* **2001**, *77*, 197 – 205.
[59] J. Zhang, S. Lu, X. Su, S. Fan, Q. Ma, T. Zhao, *J. CO2 Util.* **2015**, *12*, 95 – 100.
[60] P. Zhai, C. Xu, R. Gao, X. Liu, M. Li, W. Li, X. Fu, C. Jia, J. Xie, M. Zhao, X. Wang, Y.-W. Li, Q. Zhang, X.-D. Wen, D. Ma, *Angew. Chem. Int. Ed.* **2016**, *55*, 9902 – 9907; *Angew. Chem.* **2016**, *128*, 10056 – 10061.
[61] H. Wang, Y. Yang, J. Xu, H. Wang, M. Ding, Y. Li, *J. Mol. Catal. A* **2010**, *326*, 29 – 40.
[62] T. Li, H. Wang, Y. Yang, H. Xiang, Y. Li, *J. Energy Chem.* **2013**, *22*, 624 – 632.
[63] J. Lee, W. Chern, M. Lee, T. Dong, *Can. J. Chem. Eng.* **1992**, *70*, 511 – 515.
[64] L. Falbo, M. Martinelli, C. G. Visconti, L. Lietti, P. Forzatti, C. Bassano, P. Deiana, *Ind. Eng. Chem. Res.* **2017**, *56*, 13146 – 13156.
[65] X. Wang, J. Zhang, J. Chen, Q. Ma, S. Fan, T. Zhao, *Chin. J. Chem. Eng.* **2018**, *26*, 761 – 767.
[66] R. E. Owen, P. Plucinski, D. Mattia, L. Torrente-Murciano, V. P. Ting, M. D. Jones, *J. CO2 Util.* **2016**, *16*, 97 – 103.
[67] R. Satthawong, N. Koizumi, C. Song, P. Prasassarakich, *J. CO2 Util.* **2013**, *3 – 4*, 102 – 106.
[68] R. Satthawong, N. Koizumi, C. Song, P. Prasassarakich, *Catal. Today* **2015**, *251*, 34 – 40.
[69] T. Numpilai, T. Witoon, N. Chanlek, W. Limphirat, G. Bonura, M. Chareonpanich, J. Limtrakul, *Appl. Catal. A* **2017**, *547*, 219 – 229.
[70] T. Riedel, M. Claeys, H. Schulz, G. Schaub, S.-S. Nam, K.-W. Jun, M.-J. Choi, G. Kishan, K.-W. Lee, *Appl. Catal. A* **1999**, *186*, 201 – 213.
[71] J. Liu, A. Zhang, M. Liu, S. Hu, F. Ding, C. Song, X. Guo, *J. CO2 Util.* **2017**, *21*, 100 – 107.
[72] L. Torrente-Murciano, R. S. L. Chapman, A. Narvaez-Dinamarca, D. Mattia, M. D. Jones, *Phys. Chem. Chem. Phys.* **2016**, *18*, 15496 – 15500.
[73] J. Zhang, X. Su, X. Wang, Q. Ma, S. Fan, T.-S. Zhao, *React. Kinet. Mech. Catal.* **2018**, *124*, 575 – 585.
[74] H. Furukawa, K. E. Cordova, M. O'Keeffe, O. M. Yaghi, *Science* **2013**, *341*, 1230444.
[75] S. Hu, M. Liu, F. Ding, C. Song, G. Zhang, X. Guo, *J. CO2 Util.* **2016**, *15*, 89 – 95.
[76] A. Ramirez, L. Gevers, A. Bavykina, S. Ould-Chikh, J. Gascon, *ACS Catal.* **2018**, *8*, 9174 – 9182.
[77] S. Gupta, V. K. Jain, D. Jagadeesan, *ChemNanoMat* **2016**, *2*, 989 – 996.
[78] D. Haag, H. H. Kung, *Top. Catal.* **2014**, *57*, 762 – 773.
[79] M. Hu, Z. Yao, X. Wang, *Ind. Eng. Chem. Res.* **2017**, *56*, 3477 – 3502.
[80] Y. Cheng, J. Lin, K. Xu, H. Wang, X. Yao, Y. Pei, S. Yan, M. Qiao, B. Zong, *ACS Catal.* **2016**, *6*, 389 – 399.
[81] Y. Cheng, J. Lin, T. Wu, H. Wang, S. Xie, Y. Pei, S. Yan, M. Qiao, B. Zong, *Appl. Catal. B* **2017**, *204*, 475 – 485.
[82] J. A. Loiland, M. J. Wulfers, N. S. Marinkovic, R. F. Lobo, *Catal. Sci. Technol.* **2016**, *6*, 5267 – 5279.
[83] M. Ding, Y. Yang, B. Wu, Y. Li, T. Wang, L. Ma, *Appl. Energy* **2015**, *160*, 982 – 989.
[84] T. Riedel, H. Schulz, G. Schaub, K. W. Jun, J. S. Hwang, K. W. Lee, *Top. Catal.* **2003**, *26*, 41 – 54.
[85] X. Nie, H. Wang, M. J. Janik, Y. Chen, X. Guo, C. Song, *J. Phys. Chem. C* **2017**, *121*, 13164 – 13174.
[86] X. Nie, H. Wang, M. J. Janik, X. Guo, C. Song, *J. Phys. Chem. C* **2016**, *120*, 9364 – 9373.
[87] Z. Li, J. Wang, Y. Qu, H. Liu, C. Tang, S. Miao, Z. Feng, H. An, C. Li, *ACS Catal.* **2017**, *7*, 8544 – 8548.
[88] É. S. Van-Dal, C. Bouallou, *J. Cleaner Prod.* **2013**, *57*, 38 – 45.
[89] B. Anicic, P. Trop, D. Goricanec, *Energy* **2014**, *77*, 279 – 289.
[90] R. L. S. C. D. Chang, W. H. Lang, *J. Catal.* **1979**, *56*, 169 – 173.
[91] U. Olsbye, S. Svelle, M. Bjrgen, P. Beato, T. V. W. Janssens, F. Joensen, S. Bordiga, K. P. Lillerud, *Angew. Chem. Int. Ed.* **2012**, *51*, 5810 – 5831; *Angew. Chem.* **2012**, *124*, 5910 – 5933.
[92] S. Xu, Y. Zhi, J. Han, W. Zhang, X. Wu, T. Sun, Y. Wei, Z. Liu, *Adv. Catal.* **2017**, *61*, 37 – 122.
[93] P. Gao, S. Dang, S. Li, X. Bu, Z. Liu, M. Qiu, C. Yang, H. Wang, L. Zhong, Y. Han, Q. Liu, W. Wei, Y. Sun, *ACS Catal.* **2018**, *8*, 571 – 578.
[94] P. Tian, Y. Wei, M. Ye, Z. Liu, *ACS Catal.* **2015**, *5*, 1922 – 1938.
[95] X. Liu, M. Wang, C. Zhou, W. Zhou, K. Cheng, J. Kang, Q. Zhang, W. Deng, Y. Wang, *Chem. Commun.* **2018**, *54*, 140 – 143.
[96] M. Fujiwara, T. Satake, K. Shiokawa, H. Sakurai, *Appl. Catal. B* **2015**, *179*, 37 – 43.
[97] Y. N. Gao, S. Liu, Z. Zhao, H. C. Tao, Z. Y. Sun, *Acta Phys.-Chim. Sin.* **2018**, *34*, 858 – 872.
[98] S. Dang, P. Gao, Z. Liu, X. Chen, C. Yang, H. Wang, L. Zhong, S. Li, Y. Sun, *J. Catal.* **2018**, *364*, 382 – 393.
[99] C. Jia, W. Fan, X. Cheng, X. Zhao, H. Sun, P. Li, N. Lin, *Phys. Chem. Chem. Phys.* **2014**, *16*, 7538 – 7547.
[100] K. Sun, Z. Fan, J. Ye, J. Yan, Q. Ge, Y. Li, W. He, W. Yang, C. Liu, *J. CO2 Util.* **2015**, *12*, 1 – 6.
[101] O. Martin, A. J. Martín, C. Mondelli, S. Mitchell, T. F. Segawa, R. Hauert, C. Drouilly, D. Curulla-Ferré, J. Pérez-Ramírez, *Angew. Chem. Int. Ed.* **2016**, *55*, 6261 – 6265; *Angew. Chem.* **2016**, *128*, 6369 – 6373.
[102] D. Mores, E. Stavitski, M. H. F. Kox, J. Kornatowski, U. Olsbye, B. M. Weckhuysen, *Chem. Eur. J.* **2008**, *14*, 11320 – 11327.
[103] Y. K. Park, K. C. Park, S. K. Ihm, *Catal. Today* **1998**, *44*, 165 – 173.
[104] W. Wu, W. Guo, W. Xiao, M. Luo, *Fuel Process. Technol.* **2013**, *108*, 19 – 24.
[105] Z. Li, J. Martínez-Triguero, P. Concepción, J. Yu, A. Corma, *Phys. Chem. Chem. Phys.* **2013**, *15*, 14670 – 14680.
[106] J. Chen, X. Wang, D. Wu, J. Zhang, Q. Ma, X. Gao, X. Lai, H. Xia, S. Fan, T. S. Zhao, *Fuel* **2019**, *239*, 44 – 52.
[107] K. Larmier, W. C. Liao, S. Tada, E. Lam, R. Verel, A. Bansode, A. Urakawa, A. Comas-Vives, C. Copéret, *Angew. Chem. Int. Ed.* **2017**, *56*, 2318 – 2323; *Angew. Chem.* **2017**, *129*, 2358 – 2363.
[108] M. Zhang, Y. Wu, M. Dou, Y. Yu, *Catal. Lett.* **2018**, *148*, 2935 – 2944.
[109] L. C. Grabow, M. Mavrikakis, *ACS Catal.* **2011**, *1*, 365 – 384.
[110] I. M. Dahl, S. Kolboe, *J. Catal.* **1996**, *161*, 304 – 309.
[111] M. Bjørgen, S. Svelle, F. Joensen, J. Nerlov, S. Kolboe, F. Bonino, L. Palumbo, S. Bordiga, U. Olsbye, *J. Catal.* **2007**, *249*, 195 – 207.
[112] I. M. Dahl, S. Kolboe, *Catal. Lett.* **1993**, *20*, 329 – 336.
[113] I. M. Dahl, S. Kolboe, *J. Catal.* **1994**, *149*, 458 – 464.
[114] S. Svelle, F. Joensen, J. Nerlov, U. Olsbye, K. P. Lillerud, S. Kolboe, M. Bjørgen, *J. Am. Chem. Soc.* **2006**, *128*, 14770 – 14771.
[115] C. J. Bertole, C. A. Mims, G. Kiss, *J. Catal.* **2002**, *210*, 84 – 96.
[116] C. Yang, H. Zhao, Y. Hou, D. Ma, *J. Am. Chem. Soc.* **2012**, *134*, 15814 – 15821.
[117] A. K. Dalai, B. H. Davis, *Appl. Catal. A* **2008**, *348*, 1 – 15.
[118] J. Gaube, H. F. Klein, *Appl. Catal. A* **2008**, *350*, 126 – 132.
[119] M. Kazemimoghadam, T. Mohammadi, *Desalination* **2010**, *255*, 196 – 200.
[120] M. P. Rohde, D. Unruh, G. Schaub, *Catal. Today* **2005**, *106*, 143 – 148.
[121] S. C. Lee, J. S. Kim, W. C. Shin, M. J. Choi, S. J. Choung, *J. Mol. Catal. A* **2009**, *301*, 98 – 105.
[122] Z. Li, J. Martínez-Triguero, J. Yu, A. Corma, *J. Catal.* **2015**, *329*, 379 – 388.
[123] M. C. Alvarez-Galvan, N. Mota, M. Ojeda, S. Rojas, R. M. Navarro, J. L. G. Fierro, *Catal. Today* **2011**, *171*, 15 – 23.
[124] S. Perathoner, G. Centi, *ChemSusChem* **2014**, *7*, 1274 – 1282.

[125] G. Centi, G. Iaquaniello, S. Perathoner, *ChemSusChem* **2011**, *4*, 1265 – 1273.
[126] R. Terwel, J. Kerkhoven, *Carbon Neutral Aviation with Current Engine Technology: The Take-Off of Synthetic Kerosene Production in The Netherlands*, **2018**.
[127] K. Zeng, D. Zhang, *Prog. Energy Combust. Sci.* **2010**, *36*, 307 – 326.
[128] M. Bodner, A. Hofer, V. Hacker, *WIREs Energy Env.* **2015**, *4*, 365 – 381.
[129] T. L. Gibson, N. A. Kelly, *Int. J. Hydrogen Energy* **2008**, *33*, 5931 – 5940.
[130] Ö. F. Selamet, F. Becerikli, M. D. Mat, Y. Kaplan, *Int. J. Hydrogen Energy* **2011**, *36*, 11480 – 11487.
[131] A. Wood, H. He, T. Joia, M. Krivy, D. Steedman, *J. Electrochem. Soc.* **2016**, *163*, F327 – F329.
[132] M. Ni, M. K. H. Leung, D. Y. C. Leung, *Int. J. Hydrogen Energy* **2008**, *33*, 2337 – 2354.
[133] M. Kopp, D. Coleman, C. Stiller, K. Scheffer, J. Aichinger, B. Scheppat, *Int. J. Hydrogen Energy* **2017**, *42*, 13311 – 13320.
[134] *HyBalance—towards Carbon-Free Hydrogen*, can be found under https://www.airliquide.com/magazine/hybalance-towards-carbon-free-hydrogen (accessed January **2019**).
[135] IEA Energy Technology Policy Division and the UNIDO Energy and Climate Change Branch, *Technology Roadmap, Carbon Capture and Storage in Industrial Applications*, **2011**, https://webstore.iea.org/technology-roadmap-carbon-capture-and-storage-in-industrial-applications (accessed December **2018**).
[136] T. Mikunda, F. Neele, F. Wilschut, M. Hanegraaf, *A Secure and Affordable CO_2 Supply for the Dutch Greenhouse Sector*, TNO, Utrecht, **2015**, https://www.glastuinbouwnederland.nl/content/user_upload/15051.03_Rapport.pdf (accessed December **2018**).
[137] *The Linde Group—Carbon Capture and Storage*, can be found under https://www.the-linde-group.com/en/clean_technology/clean_technology_portfolio/carbon_capture_storage/index.html (accessed January **2019**).
[138] *Cryocap-CO_2 Cold Capture System—a World Premiere*, https://www.airliquide.com/magazine/cryocap-co2-cold-capture-system-unlike-any-other-in-the-world (accessed January **2019**).
[139] T. Kuramochi, A. Ramírez, W. Turkenburg, A. Faaij, *Renewable Sustainable Energy Rev.* **2013**, *19*, 328 – 347.
[140] T. Kuramochi, *CO_2 Capture in Industries and Distributed Energy Systems: Possibilities and Limitations*, PhD thesis, Utrecht University, **2011**, ISBN: 978-90-8891-278-8.
[141] A. Carpenter, *CO_2 Abatement in the Iron and Steel Industry*, https://www.usea.org/sites/default/files/012012_CO2%20abatement%20in%20the%20iron%20and%20steel%20industry_ccc193.pdf (accessed November **2018**).
[142] H. Kim, J. Lee, S. Lee, I. B. Lee, J.-H. Park, J. Han, *Energy* **2015**, *88*, 756 – 764.
[143] E. S. Sanz-Pérez, C. R. Murdock, S. A. Didas, C. W. Jones, *Chem. Rev.* **2016**, *116*, 11840 – 11876.
[144] R. Socolow, M. Desmond, R. Aines, J. Blackstock, O. Bolland, T. Kaarsberg, N. Lewis, M. Mazzotti, A. Pfeffer,, K. Sawyer, J. Siirola, B. Smit, J. Wilcox, *Direct Air Capture of CO_2 with Chemicals*, American Physical Society, **2011**, https://www.aps.org/policy/reports/assessments/upload/dac2011.pdf (accessed December **2018**).
[145] T. Mikunda, F. Neele, *Preliminary Technical Concept Assessment—the CO_2 Smart Grid*, https://www.bloc.nl/app/assets/bloc-co2-smartgrid-technical-concept-assessment.pdf (accessed November **2018**).
[146] I. Yarulina, J. Goetze, C. Gücüyener, L. Van Thiel, A. Dikhtiarenko, J. Ruiz-Martinez, B. M. Weckhuysen, J. Gascon, F. Kapteijn, *Catal. Sci. Technol.* **2016**, *6*, 2663 – 2678.
[147] J. E. P. Navalho, J. M. C. Pereira, J. C. F. Pereira, *AIChE J.* **2018**, *64*, 578 – 594.
[148] J. E. Sutton, J. M. Lorenzi, J. T. Krogel, Q. Xiong, S. Pannala, S. Matera, A. Savara, *ACS Catal.* **2018**, *8*, 5002 – 5016.
[149] P. J. Bereciartua, Á. Cantín, A. Corma, J. L. Jordá, M. Palomino, F. Rey, S. Valencia, E. W. Corcoran, Jr., P. Kortunov, P. I. Ravikovitch, A. Burton, C. Yoon, Y. Wang, C. Paur, J. Guzman, A. R. Bishop, G. L. Casty, *Science* **2017**, *358*, 1068 – 1071.

Manuscript received: April 3, 2019
Revised manuscript received: May 31, 2019
Accepted manuscript online: June 5, 2019
Version of record online: August 7, 2019